

Optimum Parameters for Laser-launching Objects into Low Earth Orbit

Claude R. Phipps

Photonic Associates

200A Ojo de la Vaca Road

Santa Fe, New Mexico, 87505, USA

James P. Reilly

Northeast Science and Technology

117 Northshore Blvd

East Sandwich, MA 02537, USA

Jonathan W. Campbell

NASA Marshall Spaceflight Center

MSFC, AL 35812, USA

Abstract

We derive optimum values of parameters for laser-driven flights into low-Earth orbit using an Earth-based laser, as well as sensitivity to variations from the optima. These parameters are the ablation plasma exhaust velocity v_E and specific ablation energy Q^* , plus related quantities such as momentum coupling coefficient C_m and the pulsed or CW laser intensity which must be delivered to the ablator to produce these values. Different optima are found depending upon whether it is desired to maximize mass m delivered to LEO, maximize the ratio m/M of orbit to ground mass, or minimize cost in energy per gram delivered. While it is not within the scope of this report to provide an engineered flyer design, a notional, cone-shaped flyer is described to provide a substrate for the discussion and flight simulations. The flyer design emphasizes conceptually and physically separate functions of light collection at a distance from the laser source, light concentration on the ablator, and autonomous steering. Approximately ideal flight paths to LEO are illustrated beginning from an elevated platform. We believe LEO launch costs can be reduced 100-fold in this way. Sounding rocket cases, where the only goal is to momentarily reach a certain altitude starting from near sea level, are also discussed. Nonlinear optical constraints on laser propagation through the atmosphere to the flyer are briefly considered.

1. Introduction

The way we now send things to space is very expensive. Present day costs of raising mass from the Earth's surface into low Earth orbit (LEO) with chemical rockets is more than \$10,000/kg [Table 1]. This cost – equal to the cost of gold - dominates all other considerations relating to spaceflight, limiting what we consider to be possible. But it need not be so.

Forty-five years ago – even before lasers – authors were considering ground-based photonic propulsion of space vehicles (e.g., Sänger 1956). One of these early publications (Marx 1966) considered propulsion to relativistic speeds and first introduced the ablation efficiency η_{AB} which appears in Equation [4] of this article. In the early 1970's, a series of papers considered laser space propulsion by photon reaction alone (Möckel 1972a, 1972b, 1975). This mechanism is highly efficient in producing large final velocities, but very inefficient in producing thrust, so, although it is the favored method when laser energy is cheap in the future, and for cases where time is not important (e.g., solar sail propulsion), it is of limited interest for lifting payloads from the planet into LEO.

It is the task of lifting payloads to LEO which forms the economic basis for all other space activities.

In 1972, Kantrowitz suggested using remotely generated laser power to heat a propellant sufficiently to produce a vapor or plasma jet for thrust, which is the principle of laser ablation space propulsion.

In the past decade, several publications have appeared [for example, Myrabo and Raizer 1994; Myrabo *et al.* 1998] describing an air-breathing, laser-driven aerospike flyer or "Lightcraft". This flyer has a very specific design featuring light concentration near the rim of a frisbee-like shape that provides thrust from laser supported detonations in air. It has a large diameter to length ratio (D/L) and is a free (not wire-guided) flyer [Myrabo *et al.* 1989]. Myrabo, as well as Bohn *et al* [Bohn 1999] have actually flown small "Lightcraft" devices to altitudes of 10 – 30m using tens-of-kW lasers. Recently, Myrabo flew a free-flying, pure-ablation flyer to 39 meters [Myrabo 1999]. A concern with this design is damage to the metallic reflector surface due to the close proximity of hot, dense plasma.

Bohn's flyer is presently a wire-guided, parabolic reflector which has the advantage of substantially separating the air plasma which forms at the parabolic focus from the surface of the light-collecting reflector. Bohn states that erosion of the reflector after many flights was negligible.

Phipps *et al.* (1996) and Campbell (1996) discussed a laser space propulsion concept dubbed *ORION* capable of clearing near-earth space of 1–10-cm debris using a ground-based laser in two years.

Phipps and Michaelis (1994) showed that there is an optimum set of parameters for laser space propulsion which can reduce the cost of lifting mass to LEO 100-fold.

The present article is a more complete treatment of the problem of optimizing the performance of laser-driven Earth-to-LEO spacecraft. We adopt a broad perspective, relatively free from the limitations of a specific design. In particular, we consider the three basic functions of light collection, light concentration and steering to be conceptually and physically separate, so that each can be optimized without arbitrary

February 10, 2001 edition

limits arising from coupling to the other functions. We conclude that trajectories exist, for reasonable spacecraft shapes launched from near the Earth's surface through the atmosphere to LEO, for which figures of merit are near the vacuum values, many times better than the mass ratios currently realized by chemical rockets.

Of course, optimum values vary with what parameter is being optimized, and we consider three different possibilities: a) maximum mass delivered to orbit b) maximum ratio of mass delivered to orbit to initial mass and c) minimum cost in joules per gram delivered.

2. Laser Ablation Parameters

The momentum coupling coefficient C_m is defined as the ratio of target momentum $m\Delta v$ produced to incident laser pulse energy W during the ejection of laser-ablated material (the photoablation process). By convention, this ratio is expressed in mixed units:

$$C_m = \frac{m\Delta v}{W} \quad \text{dyn-s/J or dyn/W [1E-5 N-s/J].} \quad [1]$$

In the ablation process, Q^* joules of laser light are consumed to ablate each gram of target material [$\Delta m = M - m$]

$$Q^* = \frac{W}{\Delta m} \quad \text{J/g [1E-3 J/kg]} \quad [2]$$

For a monoenergetic exhaust stream, given these definitions, and since $m\Delta v = \Delta m v_E$, momentum conservation requires the product of C_m and Q^* to be the effective exhaust velocity v_E of the laser rocket, independent of the efficiency with which laser energy is absorbed. This is simply related to the specific impulse I_{sp} :

$$C_m Q^* = v_E = g I_{sp} \quad \text{cm/s.} \quad [3]$$

In the following, we will describe a monoenergetic exhaust stream with velocity v_E . Real exhaust streams have a velocity distribution, and the error associated with the monoenergetic approximation is discussed in Appendix III. Using this approximation will not introduce large errors for laser-produced plasmas, and the results will be easy to understand.

Conservation of energy prevents C_m and Q^* from being mutually independent variables. Increasing one decreases the other. Using Eq. [3], we see that several constant product relationships exist:

$$2E7 \eta_{AB} = \Delta m v_E^2 / W = C_m^2 Q^* = g C_m I_{sp} = C_m v_E. \quad [4]$$

In Eq. [4], $\eta_{AB} \leq 1$ is the efficiency with which laser energy W is converted into exhaust kinetic energy, and the factor 1E7 is due to the units in which the quantities are defined. Symbols used in this paper are listed and defined in the glossary, Appendix I.

Choosing combinations of C_m and Q^* which exceed the limit expressed in Eq. [4] violates physics – and the errors involved in the monoenergetic approximation underestimate η_{AB} (Appendix III).

The rate of mass usage is

$$-\dot{m} = \frac{P}{Q^*} \quad [5]$$

When considering C_m and Q^* as design variables it is important to realize that the lifetime of the ablator increases with Q^* and decreases very rapidly with increasing C_m . Writing β for the acceleration “G” ratio PC_m/Mg at liftoff, some of the factors that affect ablator lifetime are shown in Eq. [6], where the final term emphasizes the crucial importance of I_{sp} :

$$\tau_{AB} = \left| \dot{m}/M \right| = \frac{MQ^*}{P} = \frac{2E7 \eta_{AB} M}{PC_m^2} = I_{sp}/\beta \quad [6]$$

In particular, increasing C_m to get more lifting power at launch through the relationship

$$F \equiv -\dot{m} v_E = -\dot{m} g I_{sp} = PC_m \equiv \beta Mg \quad [7]$$

with a fixed laser power entails a serious penalty for ablator lifetime, since, from Eq. [6], $\tau_{AB} \propto 1/C_m^2$. More mass can be lifted with high C_m , but the ablator may be used up before reaching orbit (or the end of the mission).

For times long enough for thermalization to occur (tens of ns), the exhaust velocity can be estimated from the most probable ion thermal velocity and related to the temperature of ions with average mass M_A amu:

$$v_E \approx v_{thi} = \sqrt{2kT_i/m_i} = 9.83E5 \sqrt{T_{i(eV)}/M_A} \quad [8]$$

The ion temperature which will result from laser irradiation depends on whether that radiation is pulsed or continuous (CW), and on other parameters. Table 2 shows how these expressions interrelate to give the laser ablation parameters. Putting aside how that temperature is produced, we can use Eq. [8] to estimate the temperature required to produce a given exhaust velocity. And, once that is determined, Eqs. [3] and [4] give the coupling coefficient, Q^* and I_{sp} .

We can learn several things from Table 2. C_m and Q^* values listed are the largest possible values given the listed v_E , since η_{AB} may be <1 . Anything larger than an exhaust velocity of 5E5 cm/s is definitely the result of plasma regime, because at the temperatures listed in the second column, the ionization fraction must be ≈ 1 . Such conditions are necessarily produced by a pulsed rather than a CW laser. Accordingly, throughout this work, we will assume the laser is repetitively pulsed rather than CW whenever such v_E values are applied. It should be emphasized that this is not to say that CW lasers have no place in laser launching; only that the above limits must be taken into account. In particular, Figure A4.3 is done only for a repetitively-pulsed laser, and does not consider whole-beam thermal blooming in an adequate fashion for the CW case.

Since the maximum specific impulse of ordinary chemical rockets is about 500s, limited by the temperatures available in chemical reactions, exit velocity $v_E > 5E5$ ($I_{sp} > 500s$) is accessible only by laser ablation or some other non-chemical process such as ion drives. Specific impulse I_{sp} up to 7500s has been measured in KrF-laser ablation of aluminum [Phipps and Michaelis 1994, Figure 3]. The last two columns of Table 2 give the incident pulse intensity and fluence required to generate the temperature in column 2 for a 1.06- μ m laser operating on a C-H target with an average ion mass $M_A = 6$ amu and

February 10, 2001 edition

an ionization fraction $Z=1$. The fluence listed is for a 10-ns duration pulse. That high velocities $>5E5$ cm/s are difficult to produce can be seen from these last two columns. That a CW laser can readily produce $v_E \leq 2E5$ can also be seen.

The pulsed laser parameters in Table 2 are based on the following relationship from Phipps *et al* 1988:

$$T_e = 2.57 \frac{Z^{3/4}}{(Z + 1)^{5/8}} (I\lambda \sqrt{\tau})^{1/2} \text{ eV} \quad [9]$$

In that work, pressure, temperature and mass ablation rate are derived from inertial confinement fusion concepts for a 1-dimensional laser interaction with an opaque surface in vacuum. Z is the average ionization state in the absorbing region near the critical-density surface (usually about 1).

What is Optimum?

From the foregoing discussion, it is clear that there may be optimum values of C_m , Q^* and their product v_E for launch into LEO, given a desired outcome. The three outcomes we will evaluate in this article are:

- a) Lowest possible cost $C = W/m$ (J/g) of mass delivered to LEO
- b) Maximum mass m delivered to LEO independent of cost C and ground mass M , and
- c) Maximum ratio m/M of mass surviving to LEO to ground mass M , independent of cost

Cases b) and c) are important when energy cost on the ground is less important than the mass delivered to orbit, as when the goal is to deliver the first kg to LEO, whereas a) is important when cost is the dominant factor, as when the goal is to lift several tonnes.

Variables we will consider are C_m , Q^* , v_E , launch altitude H_0 , initial velocity v_0 , initial acceleration β , and some variations in zenith angle during the flight. Because v_E depends on laser parameters like I and τ , we have the luxury of picking whatever v_E we want for a laser-driven rocket, within reason, via system design. The fundamental variable is v_E .

In the next sections, we will consider how to calculate the optimum v_E for each of the situations we face in the present task, as well as what values of C_m and Q^* are experimentally justified.

3. Optimization Including Vacuum, Gravity

For launch analysis (but not for simulation) we idealize flights as being composed of two separable segments: a vertical flight to near LEO altitude, with engine cutoff at time t_c , and a horizontal orbit insertion segment ending at time t_l . The two segments may be separated by a brief coasting interval prior to engine reignition at a turning time t_T , chosen to attain $v_r = 0$ at time t_l . Appendix V gives a detailed discussion of these points, and Figure A5.1 shows results of a simulation of such an “elbow” flight path, to demonstrate that it is not unrealistic.

Laser ablation thrust is produced by the ablation of the flyer mass $m(t)$ at a negative rate \dot{m} . The relatively small remaining vertical velocity at the turning point is [App. V]:

$$v_{rT} = -v_E \ln\left(\frac{m_T}{M}\right) - gt_T \text{ cm/s,} \quad [11a]$$

February 10, 2001 edition

and the mass ratio at the turning point is

$$\frac{m_T}{M} = \exp \left[-\left(\frac{v_{rT} + gt_T}{v_E} \right) \right] \quad [11b]$$

In vacuum, the mass ratio at orbit insertion is:

$$\frac{m_I}{M} = \Gamma \exp \left[-\left(\frac{\Delta v + gt_I}{v_E} \right) \right] \quad [12]$$

In the above, M is the flyer mass at launch, m_j is the mass at event j during the flight, g the acceleration of gravity (taken constant in low Earth orbit), $\Delta v = v_I$ is the orbit insertion velocity, and $\Gamma = \Gamma(m_T/m_I, m_I/b, \beta, I_{sp})$ is a correction factor which is never larger than 1.02 in practical cases. Appendix V gives a detailed discussion of these points, and Figure V.1 shows results of a simulation of such an “elbow” flight path, to demonstrate that it is not unrealistic. Eq. [12] shows that, in vacuum, optimizations (a) – most mass delivered to orbit and (b) – the best ratio of mass in orbit to mass on the ground is achieved for $v_E = \infty$, or $C_m = 0$ [Figure 1]. To treat optimization (c) – the energy cost optimization in vacuum – we note that the laser energy W expended in the flight is, by definition,

$$W = \Delta m Q^* = \Delta m v_E / C_m \quad J \quad [13]$$

Taking $\Gamma=1$, and defining energy cost for a laser-driven flight in space as joules per gram of mass delivered at the end of mission:

$$C = \frac{W}{m_I} = \left[\frac{(1-m_I/M)}{(m_I/M)} \right] Q^* = \frac{v_E}{C_m} \left[\exp \left(\frac{\Delta v + gt_I}{v_E} \right) - 1 \right] \quad . \quad [14]$$

There is an optimum exhaust velocity v_E for which the cost C is minimized. To find it, let $x = v_E$, $b = 2E7 \eta_{AB}$, and $a = (\Delta v + gt_I)$, so that Eq. [14] becomes

$$\frac{a}{x} = -\ln \left[1 - \frac{a}{2x} \right] \quad [15]$$

Then setting $dC/dx = 0$ gives an optimum value of a/x :

$$C = \frac{x^2}{b} [\exp(a/x) - 1] \quad , \quad [16]$$

a transcendental equation for which the solution is:

$$\frac{a}{x} = \left(\frac{\Delta v + gt_I}{v_E} \right) = 1.5936 \quad [17]$$

This is a result obtained for standard rockets by Möckel in 1975.

Equivalently, in the absence of gravity or for short flights to LEO such that $t_I \ll 800$ seconds [$\Delta v = 7.8$ km/s], the optimum exhaust velocity $v_E = 0.63 \Delta v = 4.9$ km/s.

Given Eq. [5], the corresponding coupling coefficient for optimum energy cost in this circumstance is $C_{mopt} = 41\eta_{AB}$ dyn-s/J. These conditions can be achieved by temperatures producible by both cw and pulsed lasers [Table 2].

February 10, 2001 edition

From Eq.[12], the payload ratio at this optimum a/x is $m_f/M = 0.203$, however long the flight takes, so long as $(\Delta v + g t_f) > 0$ and bearing in mind that v_E and energy cost both increase as t increases to maintain a/x at its optimum value. For comparison, m_f/M for the Shuttle is 0.0479, considering the entire Shuttle plus a 55,000 lb. payload delivered to 200km altitude as the mass m . Considering just the 55,000 lb. payload, m_f/M is only 0.013.

Figure 1 shows how the Eq. [12] predictions vary with flight time. Struggling against gravity (without considering the atmosphere), chemical rocket flights to LEO that are more than a few minutes in duration cause the ratio m_f/M to suffer badly. Only with the high exit velocities possible with pulsed laser ablation propulsion is it possible to overcome this problem. Further, with large v_E , the ratio m_f/M approaches unity. With more mass delivered, it is clear that the cost per gram delivered will decrease. Note that Eq. [4] shows that $C_m v_E$ and $C_m^2 Q^*$ are both constant products, so this desirable high v_E is obtained with modest values of C_m , and modest values of C_m correspond to large Q^* .

If the number of flights per day is in the range 1 – 5, the cost to LEO drops below \$100/kg even with the cost of building and operating a large laser facility [Phipps & Michaelis 1994]. This is a 100-fold reduction in Earth-to-LEO cost relative to present launch methods.

Figure 2 shows the predictions of Eq. [14], illustrating how steeply the cost penalty rises on the low side of the optimum value for v_E , and how the optimum shifts to larger v_E for longer flights. Figure 3 shows the same predictions, converted to variation with C_m using Eq. [4] for unit ablation efficiency. Figure 4 shows how cost varies with v_E in the absence of gravity for values of mission Δv ranging from 100m/s to 20km/s. In this Figure, the corresponding values of C_m for unit ablation efficiency are shown on the upper horizontal axis. In all cases, the minimum cost line is that given by Eq. [17].

Table 3 summarizes the main results of Figures 2 and 3 in tabular form. Note that the $C_{m\text{opt}}$ values listed are maximum values, not only optima. Smaller values than these are possible, even likely in practical situations where $\eta_{AB} < 1$, but larger C_m 's are not permitted by conservation of energy, given the exit velocities listed. Exit velocity is the fundamental variable.

4. Optimization Including Earth's Atmosphere

Figures 1–3 show that low velocity to orbit entails a dramatic penalty for mass delivery and energy cost, especially for chemical rockets. On the other hand, high velocity in the atmosphere leads to unacceptable drag losses. So, there is an additional optimum to find – for velocity – at least in the lower atmosphere. Our goal is to determine an optimum velocity profile which will produce flights close to the vacuum values for m , m_f/M , and $C = m_f/W$, even after going through the atmosphere.

Since this is a nearly infinite parameter space, it is necessary to look for a guide to help choose laser flight parameters, taking best account of atmospheric drag.

To develop this guide, we created an analytic optimization that includes the exponential atmosphere and fixed drag coefficients (simulations were not so restricted). Its results indicate higher exhaust velocities and smaller coupling coefficients for the

February 10, 2001 edition

atmospheric portion of the flight, relative to the vacuum values. We tried those values in the simulations, and found that they work. It should be repeated that pulsed lasers will often be required to achieve the peak intensity required to produce these higher exhaust velocities (Table 2). We also note that the simulation is much more precise than the analytic optimization, including, e.g., real variation of atmospheric density and temperature with height and a varying rather than a constant drag coefficient [Appendix II].

Once more, in the analysis, we separate the problem into vertical and horizontal segments. We have previously treated optimization of the horizontal part. For the vertical part which traverses the atmosphere, the equation of motion is:

$$\dot{v} = \ddot{x} = \frac{PC_m}{m} - g - \frac{C_d A \rho v^2}{m} \quad [18]$$

where P is average laser power in watts, A is the frontal projected area of the flyer and

$$\rho = \rho_o e^{-x/H} \quad [19]$$

is the variation of atmospheric mass density (g/cm^3) with altitude x and scale height H . Because at least m , β and v are functions of time and position, this is a highly nonlinear differential equation. To get a solution, we consider the case in which the laser power P is programmed to produce an acceleration proportional to the remaining mass,

$$PC_m - mg = \beta_a mg \quad [20]$$

with $\beta_a > 0$. Then the EOM becomes

$$\dot{v} = \ddot{x} = \beta_a g - \frac{C_d A \rho v^2}{m} \quad [21]$$

Without drag, this case would represent constant acceleration. A good trial solution for velocity is:

$$v = v_o e^{x/2H} \quad [22]$$

so that

$$\rho v^2 = \rho_o v_o^2 = \text{constant} \quad , \quad [23]$$

$$x = 2H v_o e^{x/2H} + x_o \quad [24]$$

and

$$\dot{v} = \frac{v_o^2}{2H} e^{x/H} \quad . \quad [25]$$

Then the remaining mass at altitude x is an integral involving the function $\beta_a(x)$

$$m = M - \int_0^f \frac{(\beta_a + 1) m g}{v v_E} dx \quad [26]$$

February 10, 2001 edition

where it is understood that m , v and β are all functions of time and position. It remains to find the function $\beta(x)$ that, together with [22], satisfies [21]. A reasonable solution occurs if we force $\beta_a(x)$ as follows:

$$g \beta_a(x) \equiv \frac{v_o^2}{2H} e^{x/H} + \frac{C_d A}{m(x)} \rho_o v_o^2 \quad [27]$$

$$v_o \equiv C_d A \rho_o v_o^2 = \alpha M g, \quad \alpha \ll 1 \quad [28]$$

In other words, we can choose a particular driving function $\beta_a(x)$ to produce a velocity profile such that the drag force $C_d A \rho v^2$ is a fixed fraction of the takeoff weight throughout the flight, velocity increasing as the atmosphere becomes thinner. We then define the problem as that of finding the optimum fraction α . This remains a very complex problem, and we cannot claim that this prescription is the best of all prescriptions. We do claim that it gives flights through the atmosphere that are not far from the optimum vacuum values, as will be seen.

There is a solution to [21] in the form

$$\beta_a(x) = \alpha \left\{ \frac{M}{C_d A \rho_o} \left(\frac{e^{x/H}}{2H} \right) + \frac{M}{m} \right\} \quad [29]$$

We now find the value of α which will minimize Δm on going through the atmosphere to a height $x = 4H$. Once through the atmosphere, we can use the vacuum optimization developed earlier. Starting from [26],

$$\Delta m = -\frac{g}{v_o v_E} \int_0^{x_f} dx e^{-x/2H} m(x) [\beta_a(x) + 1] \quad [30]$$

$$\begin{aligned} &= \frac{g}{v_o v_E} \left\{ -2H M \left[e^{-x_f/2H} - 1 \right] + \frac{v_o^2}{g} M \left[e^{+x_f/2H} - 1 \right] - \frac{2H C_d A \rho_o v_o^2}{g} \left[e^{-x_f/2H} \right. \right. \\ &\quad \left. \left. - 1 \right] \right\} \\ &= -\int_0^{x_f} dx e^{-x/2H} \Delta m - \frac{v_o^2}{2gH} \int_0^{x_f} dx e^{+x/2H} \Delta m \end{aligned}$$

Eq. [30] is an integral equation which can be simplified and summarized:

$$\Delta m = \mathcal{O} + b \int_0^f \Delta m e^{-ax} dx + d \int_0^f \Delta m e^{+ax} dx \quad [30a]$$

and has the solution

$$\Delta m = \mathcal{O} e^{b/a} \exp \left[-\left(\frac{b}{a}\right) e^{-ax} \right] e^{-d/a} \exp \left[+\left(\frac{d}{a}\right) e^{+ax} \right] \quad [31]$$

February 10, 2001 edition

where

$$a = \frac{1}{2H}, \quad b = \frac{-g}{v_o v_E}, \quad d = \frac{-v_o}{2 H v_E}$$

$$\mathcal{O} = b \left[\frac{v_o^2 M}{g} (e^{ax} - 1) - (2MH)(1 + \alpha)(e^{-ax} - 1) \right] \quad [32]$$

Note that the parameter $\alpha = C_d A \rho_0 v_o^2 / (Mg)$ in Eq. [32] contains the information about drag. Since v_o implicitly involves α , it is not worth the effort to analytically optimize [31] with respect to α . Instead, a plot of Eq. [31] – Figure 6 – shows the best value is $\alpha = 0.07$.

Figure 6 shows that initial velocity of about 100m/s, increasing exponentially as atmospheric density decreases with altitude during the launch, and initial acceleration β of about 8 G's are good choices. Note, however, that to obtain such a velocity profile, initial laser power for a 100-kg flyer is peaked at $P = (\beta+1)Mg/C_m \approx 40\text{MW}$. In practice, some divergence from the ideal profile is expected because, with a real laser, as with realistic simulations of real lasers, this peaking will not be possible – if larger power is available, it will be used. In addition, real drag coefficients are velocity dependent, and [31] does not take account of that dependence.

Figure 7 is a similar plot for the sounding rocket case, starting from 1km altitude with a 10-cm diameter flyer and running to 75-100 km. Figure 5 shows that for sounding rockets, the optimum α is not a constant, but depends strongly on the exhaust velocity chosen. The value of α is much larger, in the neighborhood of 1 rather than 0.1. That is, the optimum flight tolerates higher drag. For this case, initial velocity of 75 – 100m/s and acceleration $\beta \approx 1\text{G}$ are good choices. For this case, laser power $P = (\beta+1)Mg/C_m$ of at least 250kW is required.

Given this preamble, we will see in the simulations section that these estimates of ideal laser flight parameters are quite close to being correct.

Ablation Efficiency

Ablation efficiency can approach 100%, as direct measurements on cellulose nitrate in vacuum verify, but a value of 50% or even less is likely [Figure 5, from Phipps and Michaelis 1994]. The impact of $\eta_{AB} < 1$ is that the C_m value deduced from a given v_E may be less than the maximum permitted by conservation of energy. Exit velocity v_E is the more fundamental quantity.

How do we measure ablation efficiency? By independently and simultaneously measuring Q^* (which is done by carefully measuring mass loss) and C_m (which is done with an impulse measurement device such as a pendulum). Knowing both quantities, from the preceding theory we can determine $v_E = C_m Q^*$ and, from Eq. [5], $v_E C_m / 2E7 = \eta_{AB}$.

5. The Flyer, Flight Stability and Trajectories

For the purpose of discussion and flight simulations, we require a conceptual flyer design. We do not claim to have done a complete engineering design, which would be required before the design would be ready to fly. Our design demonstrates one feature we believe to be important: physical and conceptual separation of the functions of light collection and ablation. In this way, limitations of one function do not unnecessarily limit the other.

A cone shape was chosen for the flyer because drag coefficients are well known for that shape [see Appendix II]. This choice also facilitated optimization of diameter to length (D/L) ratio. The need for this optimization arises from the competing interests of reducing drag – minimized for a slender flyer – and maintaining the center of thrust ahead of the center of drag, a choice which leads to a short, squat shape. This is because the latter condition in a cone-shaped flyer requires locating the ablator about L/3 forward from the rear of the cone. A long and slender flyer has the problem that the motor is then so far forward that its exhaust will coat or melt the Fresnel lens. Simulations showed that $D/L \approx 1$ was a good compromise. Figure 8 shows the flyer.

We discuss a heavy and a light flyer of the type shown in Figure 8 to illustrate two extremes of launch trajectory. The heavy flyer is very efficient but requires more than one laser station along its route because of unfavorable elevation angle with respect to a single station at the end of powered flight. The light flyer is less efficient but gets to LEO quickly with good elevation angles. Mass budgets for the two flyers are given in Tables 4 and 5, respectively.

High Altitude Launch

Dramatic advantages accrue from launching laser driven rockets bound for LEO from an initial altitude of 30 – 35km [Figure 9]. One relatively inexpensive way of doing this is to use a high altitude balloon as a launch platform. Reaching 35km altitude in this way is not difficult. Balloons have been to 39 km [Murcray *et al* 1979]. NASA Godard Spaceflight Center is currently developing an Ultra Long Duration Balloon. “The ULDB will stay aloft at altitudes of up to 115,000 feet (35 kilometers) for as long as 100 days with more than a ton of scientific instruments. For some experiments, this could be cheaper than going to space, and just as effective” [NASA GSFC 1999]. The cost of lifting a tonne to an altitude of 35 km using commercial balloon services is in the range \$50k - \$150k [Pettit 1994, Golden 1995]. We only need lift <0.05 tonnes. Realistic alternatives to a balloon are a Myrabo flyer for a first stage, or a high altitude aircraft.

A smaller Lightcraft could begin at lower altitude, but this study is mainly addressed to the problem of getting 1kg or more to orbit. We will see that this implies a MW-class laser, which in turn implies an object with a light collector diameter on the order of 100 cm, in order to limit laser intensity on the collector to 150 W/cm², a level that is safe for lens materials.

For the sounding rocket case, ground launch has the highest value because the intention is to launch a small mass from the ground at minimum cost.

Steering and Stability

During flight through the atmosphere, we require that the center of thrust be ahead of the center of drag to ensure aerodynamic stability. Beyond the atmosphere, stability becomes a matter of active control with sufficient bandwidth. However, due to highly

February 10, 2001 edition

stringent weight requirements, the easy ways of doing this (such as gas jets) are prohibited.

Two elements providing orientation control are suggested. One is gimbal pointing of the ablation motor, for low-frequency control. The second element is the “Venetian blind” reflectors, which are the high-frequency steering component. These are 8- μ m-thick copper- or aluminum-flashed kapton (depending on wavelength) in lightweight frames, and can also provide significant steering inputs by biasing the temperature distribution across the face of the ablator. Control of the reflectors is by linear motors or equivalent lightweight electrically driven actuators. The actuators and microprocessor controlling them are supplied by a generator which absorbs a few kW of incident power to create a 100W dc supply for the system. Depending on laser wavelength, this generator is a photoelectric device (highly preferable for efficiency’s sake!) or a Seebeck generator or other thermoelectric device for IR wavelengths [Frederikse 1989]. In the latter case, for the short duration of the flight, the Seebeck device can dump its heat to the payload. The system is completely robotic: there is no provision for external control. In principle, at least [because a control system study was not possible within the scope of this effort], given adequate control loop bandwidth these two control mechanisms are adequate to keep the flyer engine pointed in vacuum.

6. Beam Propagation to the Flyer

Diffraction, Light Collection and Adaptive Optics

For a gaussian transverse profile beam, the spot size d_s at the target is related to beam launch optic diameter D_b , Strehl ratio S , range z and wavelength λ by [Phipps, *et al.* 1996]:

$$\frac{1}{d_s^2} = \left(\frac{\pi \sqrt{S} D_b}{4 z \lambda} \right)^2 + \frac{1}{D_b^2} \quad [33]$$

Usually, $d_s \ll D_b$, and the beam is far from gaussian, but instead uniformly fills the transmitting optic. In this case d_s be approximated via the usual Rayleigh range equation [Phipps, *et al.* 1996]:

$$d_s \approx \frac{2.44 z \lambda}{D_b \sqrt{S}} \quad [34]$$

[Eq. [34] illustrates one of the most immediate concerns in designing a laser driven flyer: being sure that d_s is smaller than the diameter of the optic d on board the flyer which collects and focuses the light on the ablating material inside it. In Eq. [34], the “Strehl ratio” S measures the fact that, even in vacuum, beams will not have the theoretical far-field intensity given by the $S=1$ diameter, but something less. In vacuum, one speaks of the beam being “ $1/\sqrt{S}$ times diffraction limited” in its diameter in the far field.]

In the far field of a beam that has passed through the atmosphere, additional distortion effects arise. The most well-known of these is scintillation due to random phase produced in the beam, which behaves as if it arose from multiple adjacent time-dependent

February 10, 2001 edition

random phase apertures of size r_o within the beam, with frequency content extending up to about 1kHz.

We can summarize the impact of turbulence [Parenti 1992, Campbell, 1996], by noting that the far field diameter acts as if it originated from a transmitting optic with diameter r_o , not D_b

and that

$$r_o \propto \lambda^{6/5} \quad [35]$$

varies slightly more rapidly than wavelength. The result is an important, but hidden, wavelength-dependence in S . Since $r_o \approx 10\text{cm}$ at a good site at $\lambda = 530\text{nm}$, we can see why amateur astronomers get nearly theoretical performance in brief exposures with telescopes having 10–20-cm diameter but no adaptive optics.

Figure 10 is meant to illustrate all the above points by showing how the spot size increases with range for 5 situations: $\lambda = 530\text{ nm}$ (doubled Nd) with and without adaptive optics (AO), $\lambda = 1.32\text{m}$ (the COIL laser wavelength) with and without AO and $\lambda = 10.6\text{m}$ (the CO₂ wavelength) without AO all using a 3.6-m diameter primary mirror and a Strehl ratio of 50%. At 10.6m, AO is not necessary because r_o has grown to nearly the size of the aperture. This is why 1.32m with no AO is worse. Actually, 11.15 m rather than 10.6m would be the wavelength of choice in the mid infrared because it can penetrate the atmosphere with very low absorption and because it is a high-gain line of the isotopic molecule ¹³C¹⁶O₂ [see Campbell, 1996].

The dashed line across the Figure at 50cm is meant to indicate that, with 3.6-m telescopes such as exist at U. S. Air Force Starfire Optical Range, Kirtland AFB, New Mexico or at the U. S. Air Force AEOS telescope on Maui, a typical operating range of 400km dictates that the laser wavelength be in the spectrum bounded by iodine (1.315m) and doubled Nd (530 nm) with adaptive optics. Figure 10 also shows that, for any reasonable combination of wavelength and telescope diameter, the lightcraft must have a collection optic once it has gone past about 80 km slant range z .

Of course, the 11.2m wavelength would work adequately for this range using some minimal AO [perhaps 30 actuators] and a 25-m diameter mirror. It would be very difficult to steer a monolithic mirror of that size at the required rate of 1 /s, but one way in which this wavelength could be used is to synthesize the 25-m aperture as a phased array.

There are other considerations such as wavefront tilt [See Phipps *et al* 1996]. The lowest order wavefront distortion for a laser beam propagating through turbulence is an average tilt which results in a pointing error. The easiest way to sense and correct this error is to view the flyer using reflected sunlight, where possible, or by actively illuminating the flyer with a secondary laser source. The tilt in the wavefront is measured by focusing the light returned from the target and collected by the telescope aperture onto a quad cell and measuring the displacement of the focal spot. The focal displacement is proportional to the tilt with the constant of proportionality being the focal length of the system. This wavefront tilt must be compared with the tracking information obtained from the target detection system in order to extract the turbulent contribution. Compared to scintillation, it is a relatively low-bandwidth phenomenon.

February 10, 2001 edition

There is also a relativistic correction. Reflected light from the target is not precisely at the correct place due to the lead angle, $2v/c$, where v is the orbital speed of the flyer and c is the speed of light. The lead angle corresponds to the distance the flyer travels in the time it takes light from the flyer to reach the ground and the laser light to return to the flyer. For low earth orbit, the lead angle is ≈ 50 mrad or ≈ 10 arcsec. By knowing the vector velocity of the flyer we can use this relationship to automatically correct for relativistic lead.

Also of importance are considerations of how delivery of the laser intensity which is required on the ablator to achieve the desired exit velocity couples with nonlinear optical effects in the atmosphere to prevent beam delivery in one way or another. These effects, primarily Stimulated Thermal Rayleigh Scattering and Stimulated Raman Scattering (STRS and SRS), are treated in Appendix IV, and shown to be a negligible problem for the beam intensities we are likely to use to launch a Lightcraft.

7. Simulated Flights to Low Earth Orbit

Launch Procedure

The following list summarizes a successful procedure for launches to LEO which gives results close to vacuum values.

- 1) Start at 30 – 35km
- 2) Initial acceleration 1 – 2G's – not more– to avoid unnecessary drag and approximate the conditions on α and β dictated by the optimization.
- 3) Start at 90° elevation angle (vertical flight) until $v_r \approx 0.3$ km/s, then gradually roll over to 50 – 60° until $v_r \approx 1.2$ km/s.
- 4) Turn off the laser, coast down to $v_r \approx 0.8$ – 0.2 km/s, depending on C_m .
- 5) Rotate flyer to horizontal
- 6) Reapply laser to reach orbit insertion with $v_r = 0$.

Illumination Geometry at Launch

Figures 11A and 11B show simulated trajectories, to scale, for the two types of flyers in order to motivate the next Figure. Figure 12 outlines the problems faced in illuminating the flyer throughout such trajectories, and the necessity for station offset appropriate to the initial trajectory elevation angle.

As illustrated in Figure 11A, given a launch profile, it is easy to adjust station offset so that the laser's angle of incidence on the flyer is zero. It is important for this angle to be small to avoid aberration of the Fresnel lens focus. A more difficult problem occurs when the flyer is rotated for orbit insertion [Figure 11B].

Results for Optimizations of LEO Flights

Illustrative results for the variation of mass, acceleration, altitude, range, incidence angle, elevation angle and drag power during the flight follow as Figures 13 – 17.

Figure 18 shows how the collection of simulated flights support the theory for optimizations a), b) and c) – that is, mass, mass ratio and cost. Mass delivered to orbit independent of the cost, optimizes at $C_m = 20$ in air. This is noticeably different from the results of vacuum theory [see discussion at Eq. [17], in that the optimum C_m has shifted to a lower value, corresponding to the requirement for a higher Q^* to permit taking more time to move through the lower atmosphere so as to avoid unacceptable drag losses. As

February 10, 2001 edition

predicted by theory, the ratio m/M is optimized for the lowest possible C_m [corresponding to the highest exhaust velocity or I_{sp}].

Figure 19 shows that the results of simulated flights compare well to vacuum cost predictions. Discrete points on this plot represent simulations using our DoOrbits code [Appendix II], in air from an initial altitude of 35 km. Conditions for the data are noted in the Figure caption.

We conclude that an auxiliary chemical rocket would not be needed to reach orbit. In fact, it would be counterproductive, since we can achieve a much higher I_{sp} with laser ablation than is possible with chemical reactions. This means that using an auxiliary chemical rocket would actually burden rather than help the flight in any of its segments. The good m/M ratios in the present study are simply not possible with chemistry.

Table 6 summarizes the features of our best simulated flights. Note that maximum mass delivered to LEO occurs when initial $\alpha = 0.02 - 0.04$, not far from the predictions of our atmospheric transit theory, even though β and v_o were constrained to somewhat non-optimum values by the conditions of the simulation.

Results for Sounding Rocket Flights

Sounding rockets are much smaller flyers than those bound for LEO which we have been discussing, whose main goal is to take a small payload to a fixed altitude once at zero final velocity, rather than reaching orbital speed. They are of interest because they may represent the first economically viable application of laser ablation propulsion. Maximum range is much less than for LEO flights, and flyer mass, laser power and flyer diameter (governed by the size of its light collection optic) are all appropriately smaller. Figures 20 and 21 show the results our simulations obtained for two sounding rocket cases where we assume the flyer diameter is 10cm, a size which is required to penetrate the lower atmosphere from sea level as efficiently as our LEO flyers did from 35 km. Note, however, [Figure 22] that the mirror diameter required to illuminate the 10-cm collecting optic on the sounding rocket at the end of powered flight (a figure which is less than the maximum altitude achieved) becomes unwieldy for a low-cost demonstration at the CO₂ laser wavelength.

8. Conclusions

Summary

We have shown analytically what optimum exhaust velocity must be for flights of from Earth to LEO in vacuum, for a simple cone-shaped flyer driven completely by laser ablation, for three different desired outcomes: minimum cost, maximum mass or maximum mass ratio delivered to low Earth orbit.

As a guide for selecting laser parameters for the initial part of the flight in air, we have developed for the first time an analytical optimization which indicates optimum initial flyer velocity and acceleration for penetrating the atmosphere while staying very close to the energy budget of a flight in vacuum.

We have shown that it does not make energetic sense to launch LEO-size craft from the ground [Figure 9], but suggest doing so from 30 – 35 km altitude using a balloon.

With optimum flight profiles, it costs about 100kJ/g to put mass in LEO. Present energy costs are about 3¢/MJ at retail on the ground. Accordingly, it ought not cost a great deal more than \$3/η per kg to reach LEO where η is the product of all efficiencies

February 10, 2001 edition

intervening between the wall plug and the kinetic energy of the laser-ablation rocket exhaust [Kantrowitz 1998]. That this cost can be as little as \$100/kg makes sense even if η is as small as 3%. Much more careful considerations of laser facility construction and operation cost in Phipps and Michaelis 1994 were used to derive this cost figure [see Figure 7 of that reference], which applies for 1 – 5 flights per day.

We have shown that a 1MW laser can deliver 6kg to low Earth orbit in about 700 s.

For sounding rockets, just 20kW can deliver 100 grams to 405 km altitude from near sea level in 1200s. This by itself is a fascinating result. Lasers of this power level are readily available. Assuming a visible wavelength laser with 10% electrical efficiency, the energy cost on the ground to achieve this is \$4.75.

Recommendations

A repetitively-pulsed laser with high average power is ideal for laser space propulsion and has been assumed throughout this work whenever $I_{sp} > 500s$ was employed. For launching 5 to 10kg into LEO, a laser with average power $\approx 1\text{MW}$ is needed. To illuminate a 1-m target at 400 to 800 km range, laser wavelength in the 1 \AA m range (not 10 \AA m) is consistent with diffraction limits set by existing beam directors.

Unfortunately , the only existing high-average-power lasers with adequate beam quality and wavelength in the 1 \AA m region are CW, not repetitively-pulsed, and this situation is unlikely to change for some time.

Rather than conclude that nothing can be done in this decade by way of a flight demonstration, Table 7 proposes parameters for a first step in laser space propulsion using a CW laser. The sounding rocket configuration is chosen to minimize range. A reasonable plan would be to use the 3.67-m-diameter “Starfire” mirror at Kirtland Air Force Base, Albuquerque, NM or its equivalent at Maui (“AEOS”), together with an 80-kW iodine laser. The spot size of the laser at maximum cutoff range is 20 cm, so 75% of its power is wasted by the time the flyer reaches maximum range. However, since the flyer spends most of its time closer than maximum range, deviations from Table 7 due to this cause will be small. The C_m and v_E values quoted in the Table are based on simulations [Reilly 1996] of CW interactions, not measurements.

Acknowledgments

The authors are grateful for useful discussions with and ideas from Mike Lander Anteon Corporation, Dayton OH, Prof. Leik Myrabo, Renssalaer Polytechnic Institute, Prof. Max Michaelis, University of Natal and Prof. (Emeritus) Arthur Kantrowitz, Dartmouth College, former head of AVCO Research Laboratory. Dr. Bill Larson, AFRL Edwards AFB is thanked for suggesting the plot which became Figure 4.

References

- AFANAS'EV, YU. V., BASOV, N.G., KROKHIN, O.N., MORACHEVSKII, N.V., and SKLIZKOV, G.V. (1969) *Sov. Phys. Tech. Phys.* **14** 669
- APOSTOL, L., VATANOV, V. A., MIKHEILESKU, I.N., MORZHAN, I., PROKHOROV, A.M., AND FEDOROV, V.B. (1976) *Sov J. Quant. Electron.* **6** 1119-20
- AUGUSTONI, A.L., ERMER, P.G., HECKLER, R. T., KUWASHIMA, G.R., MCKAY, J.A. AND RUDDER, R.R. (1986) report AFWL-TR-85-126 [Air Force Research Laboratory, Kirtland AFB, NM 87117]
- BARNARD, J. J. (1989) *Appl. Opt.* **28**, 438
- BOHN, W.,(1999), *Proc. SPIE Symposium on Advanced High Power Lasers and Applications, Institute for Laser Engineering, Osaka* [SPIE vol. 3885, pp. 48-52]
- CAMPBELL, J. W., ED. (1996) *Project ORION: Orbital Debris Removal Using Ground-Based Sensors and Lasers*, NASA Marshall Spaceflight Center Technical Memorandum 108522
- CARMAN, R. L., PENNINGTON, D. M., HENESIAN, M. A. AND HELLWARTH, R.W., (1988) *Phys. Rev. A* **39**, 3003
- CARMAN, R. L., SHIMIZU, F., WANG, C. S. AND BLOEMBERGEN, N. (1970) *Phys Rev. A* **2**, 60-72
- COMBIS, P., DAVID ,J.& NIERAT, G.(1992) *Revue Scientifique et Technique de la Defense, CEL-Valenton no.4*
- CORNARA,S., BEECH, T.W., BELLÓ-MORA, M., and DE ARAGON, A.M.,(1999), "Satellite Constellation Launch, Deployment, Replacement and End-of-life Strategies", paper SSC99-X-1, *Proceedings of AIAA Conference on Small Satellites Utah State University 1999*
- DINGUS, R. 1987 (unpublished) summarized in McKay, J. and Laufer, P., ed. *Physical Sciences, Inc. final report, contract no. N00014-86-C-2241*
- DREYFUS, R.W. (1991) *J. Appl. Phys.* **69** 1721-9
- DUZY,C., WOODROFFE, J.A., HSIA, J.C., AND BALLANTYNE, A., (1980) *Appl. Phys. Lett.* **37**, 542-4
- ERMER,P.G., HECKLER, R.T., AND RUDDER, R.R.,(1987) (unpublished) summarized in McKay, J. and Laufer, P., ed. *Physical Sciences, Inc. final report, contract no. N00014-86-C-2241*
- ERSKINE, R., NASA (1993) Office of Spaceflight, private communication. This figure is based on \$412M for cost for a Shuttle launch. Other estimates [e.g., Park 1993] range up to \$1.1B
- FREDERIKSE, H. (1989),§6 "Seebeck effect", *A Physicist's Desk Reference*, American Institute of Physics, New York, p. 310
- FULGHUM, S. F., TRAINOR, D.W.,DUZY,C. AND HYMAN, H.A. (1984) *IEEE J. Quant. Electron.* **QE-20**,218-22

- GOLDEN, ROBERT, (1995) New Mexico State University Las Cruces, NM private communication
- GRADSHTEYN, I. S. AND RYZHIK, I. M. (1965), *Table of Integrals, Series and Products*, Academic Press, New York
- GREGG, D. & THOMAS, S. J. (1966) *J. Appl. Phys.* **37** 2787-9
- HEEMAN, R. J. AND GODFRIED, H. P. (1995) *IEEE J. Quant. Electron.* **31** 358-64
- HELLWARTH, R. W. (1975) *Prog. Quant. Electron.* **5**, 1-68
- HELLWARTH, R. W. (1995) *private communication*
- HELLWARTH, R. W., PENNINGTON, D. M. AND HENESIAN, (1990) *M. A. Phys. Rev. A* **41**, 2766-2777
- HENESIAN, M. A., SWIFT, C. D. AND MURRAY, J. R. (1985) *Opt. Lett.* **10**, 565-7
- HERRING, G. C., DYER, M. J. AND BISCHEL, W. K. (1986) *Phys. Rev. A* **34**, 1944-51
- KANTROWITZ, A. (1972) *Aeronaut. Astronaut.* **10**, 74
- KANTROWITZ, A. (1998), *Proc. Santa Fe High Power Ablation Conference 1998* SPIE **3343** pp 5-9
- KELLY, R. & DREYFUS, R. W. (1988) *Nucl. Inst. Meth.* **B32**, 341
- Küper, S. & Stuke, M. (1989) *Appl. Phys. Lett.* **54**, 4-6
- KURNIT, N., ACKERHALT, J. AND WATKINS, D.E., (1987) "Stimulated Raman Scattering in the Atmosphere", Los Alamos National Laboratory Technical Memorandum LA-UR-87-97
- LENCIONI, D. E. AND KLEINMAN, H. (1975) *report AGARD -CP-183*, National Technical Information Service, Springfield VA
- MARBURGER, J.H. (1975) *Prog. Quant. Electr.* **4**, pp.35-110
- MARX, G. (1966) *Nature* **211**, 22
- MCKAY, J.A. AND LAUFER, P.M., (1987) "Survey of Laser-produced Pressure and Impulse Data" Final Report no. PSI-1012/TR-757: Physical Sciences Inc. New England Business Center, Andover MA 01810-1077 pp. 1-236
- MÖCKEL, W.E. (1972a) *J. Spacecraft and Rockets* **9**, p. 863-8
- MÖCKEL, W.E. (1972b) *J. Spacecraft and Rockets* **9**, p. 942-4
- MÖCKEL, W.E. (1975) *J. Spacecraft and Rockets* **12**, p. 700-1
- MURCRAY, D. (1979) *Geophys. Resch. Lett.* **6** 857
- MYRABO *et al.*, (1989) Final Technical Report, Contract 2073803, Lawrence Livermore National Laboratory
- MYRABO, L. N. (1999), *Proc. Santa Fe High Power Ablation Conference 2000* SPIE **4025**

- MYRABO, L. N., RAIZER, YU. P. AND SCHNEIDER, M. N.(1998), *High Temperature* **36** no. 2 pp. 287-292
- MYRABO, L.N. AND RAIZER YU. P. (1994), AIAA Plasmadynamics and Lasers Conference, Colorado Springs, Paper 94-2451
- NASA (1999) *Office of Space Flight, Code M, FY 2001 Federal Budget* [http://www.nasa.gov/budget/budget_index.html]
- NASA GSFC (1999) *press release*:
<ftp://pao.gsfc.nasa.gov/pub/PAO/Releases/1999/W99-112.htm>
- ORI, A., NATHANSON, B. AND ROKNI, M. J. (1990)*Phys. D.* **23**, 142-9
- PARENTI, R. R. (1992) *Lincoln Laboratory Journal* **5**, no. 1, p. 93-114
- PARK, R. (1993) March 26 "What's New" Online Newsbulletin, American Physical Society, Washington, DC Msg: AGJD-5778-5541
- PENNINGTON, D. M., HENESIAN, M. A., AND HELLWARTH, R. W., (1988) *Phys. Rev. A* **39** pp. 3003-3009
- PETTIT, DONALD (1994) Los Alamos National Laboratory, private communication
- PHIPPS, C. R., Friedman, H. Gavel, D. ,Murray, J. ,Albrecht, G. ,George, E. V. ,Ho, C., Priedhorsky, W., Michaelis M. M. and Reilly, J. P. (1996) "ORION: Clearing near-Earth space debris using a 20-kW, 530-nm, Earth-based, repetitively pulsed laser", *Laser and Particle Beams*, **14** (1) pp. 1-44
- PHIPPS, C.R., (1996) in Campbell (1996), Appendix D, "Analysis of the ORION System Concept", pp 147-251
- PHIPPS, C. R. AND DREYFUS, R. W. (1993) Chapter 4, "Laser ablation and plasma formation" in *Laser Microprobe Analysis*, A. Vertes, R. Gijbels and F. Adams, eds., John Wiley, NY, pp.. 369 *et seq.*
- PHIPPS, C. R., Turner, T. P. Harrison, R. F. York, G. W., Osborne, W. Z., Anderson, G. K., Corlis, X. F., Haynes, L. C., Steele, H. S., Spicochi, K. C. and King, T. R., (1988) "Impulse Coupling to Targets in Vacuum by KrF, HF and CO₂ Lasers" , *J. Appl. Phys.*, **64**, pp. 1083-96
- PHIPPS, C. R., (1993) "LISK-BROOM: A laser concept for clearing space junk," in *AIP Conference Proceedings* **318**, Laser Interaction and Related Plasma Phenomena, 11th International Workshop, Monterey, CA October, 1993, George Miley, ed. American Institute of Physics, New York (1994)pp. 466-8
- PHIPPS, C. R.,Harrison, R. F., Shimada, T., York, G. W., Turner, T. P., Corlis, X. F., Steele, H. S., Haynes L. C., and King, T. R. (1990) "Enhanced Vacuum Laser-impulse Coupling by Volume Absorption at Infrared Wavelengths", *Laser and Particle Beams*, **8**, pp. 281-297
- PHIPPS, C.R. , KING, T.R., DINGUS, R.S., YORK, G.W., OSBORNE, W.Z., HARRISON, R. F., SPICOCHI, K.C. AND STEELE, H.S., (1984) (unpublished) data cited in McKay and Laufer (1987)

- PHIPPS, C.R. AND MICHAELIS, M. M. (1994), "LISP", *J. Laser and Particle Beams* **12** no. 1, pp. 23-54
- PREUSS, S., DEMCHUK, A. AND STUKE, M. (1995) "Sub-ps UV laser ablation of metals", *Appl. Phys. A* **61**, 33-7
- PUCIK, T., AND CRAWFORD, R.C., "Optical Laser Impulse Coupling Data Package", RDA report 2.28.90 available from Logicon/R&D Associates, P.O.Box 92500, Los Angeles, CA 90009
- REILLY, J. P. 1976 *Proc. Second DoD High Energy Laser Conference*, US Air Force Academy, Colorado Springs
- REILLY, J. P. 1996 [private communication]
- ROSEN,D.I., MITTELDORF, G., KOTHANDARAMAN, G., PIRRI, A.N., and PUGH, E.R. (1982) *J. Appl. Phys.* **53** 3190-3200
- ROSEN, D.I., HASTINGS, D.E. & WEYL G.M. (1982) *J. Appl. Phys.* **53** 5882-5890
- ROSEN, NEBOLSINE & WU (1978) paper V1, *AIAA Conf. Dynamics High Power Lasers, Cambridge, MA* (unpublished) data cited in McKay and Laufer (1987)
- RUDDER, R. R. (1972)report AFWL-TR-72-243, pp. 92-6 [Air Force Research Laboratory, Kirtland AFB, NM 87117]
- RUDDER, R. R. (1974) report AFWL-TR-74-100 , pp 189-198 [Air Force Research Laboratory, Kirtland AFB, NM 87117]
- SÄNGER, E. (1956) *Aero Digest*, pp. 68-73
- SHAW, M. J., HOOKER, C. J. AND WILSON, D. C. (1990) *Opt. Commun.* **103**,153-160
- SHUI, YOUNG & REILLY, (1978) *AIAA Journal* **16** 649-50
- U.S. CONGRESSIONAL BUDGET OFFICE (1993, *Analysis of Shuttle Launch Costs*
- URSU, ET AL. (1981) *Opt. Comm.* **39** 180-185
- WATT, R.G., (1987) (unpublished) data cited in Pucik, (1990)
- WILSON, R.S. (1986) (unpublished) data cited in McKay and Laufer (1987)
- WOLFE, W.L. AND ZYSSIS G. J. (1978) *The Infrared Handbook*, Infrared Information and Analysis Center, Environmental Research Institute of Michigan, Ann Arbor, MI [Library of Congress Catalog Card No. 77-90786] p. 5-107.

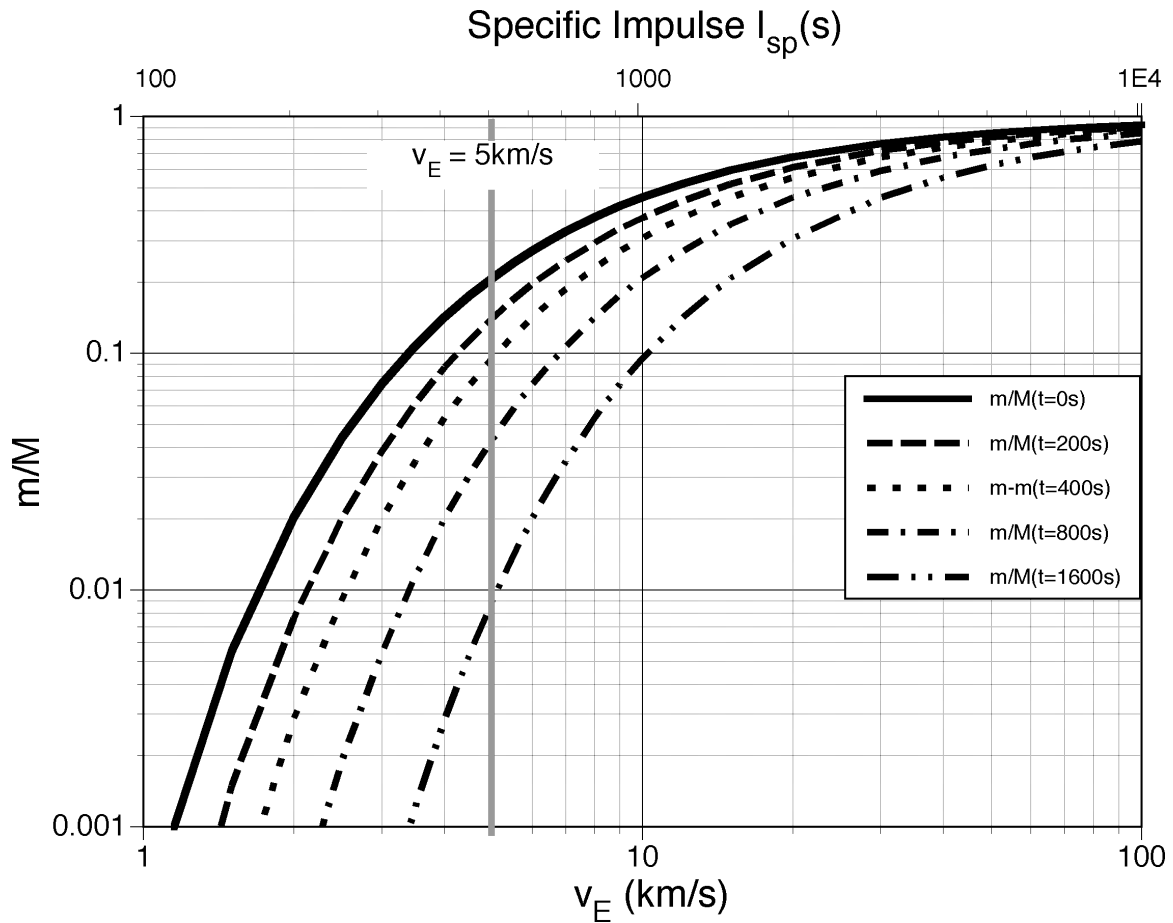


Figure 1. Ratio of mass m delivered to low Earth orbit (LEO) to initial mass M , vs. exit velocity v_E or specific impulse, in vacuum. For chemical rockets with $I_{sp} \approx 500\text{s}$, long flights are disastrous for this ratio. On the other hand, for a very hot exhaust, such as is available with laser ablation propulsion [Table 2], the ratios are very good and flight time doesn't matter very much.

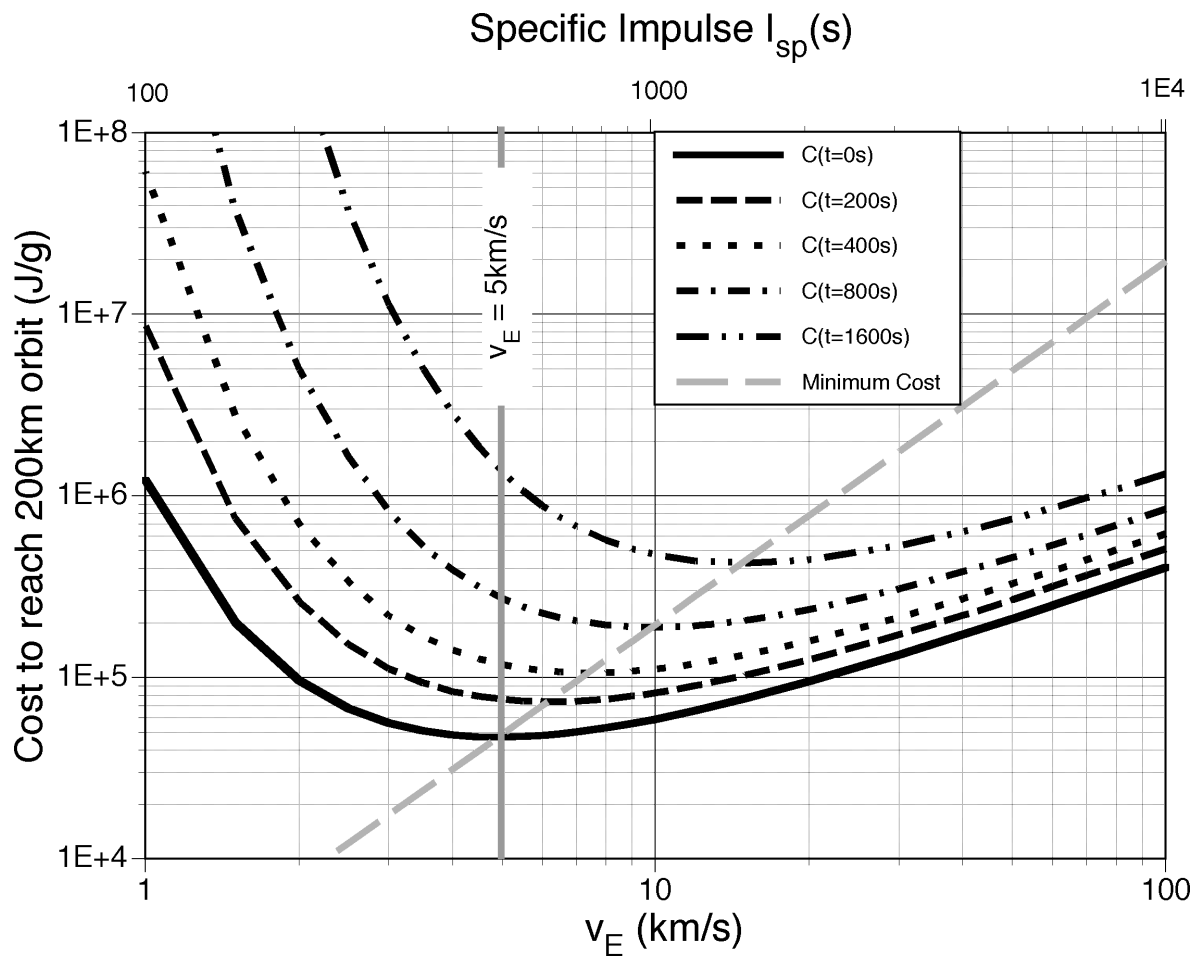


Figure 2. Cost in joules per gram delivered from the ground to a 200km altitude orbit against gravity in vacuum, versus exit velocity v_E for various flight times. Long-duration flights to LEO require high exit velocity to be cost-efficient.

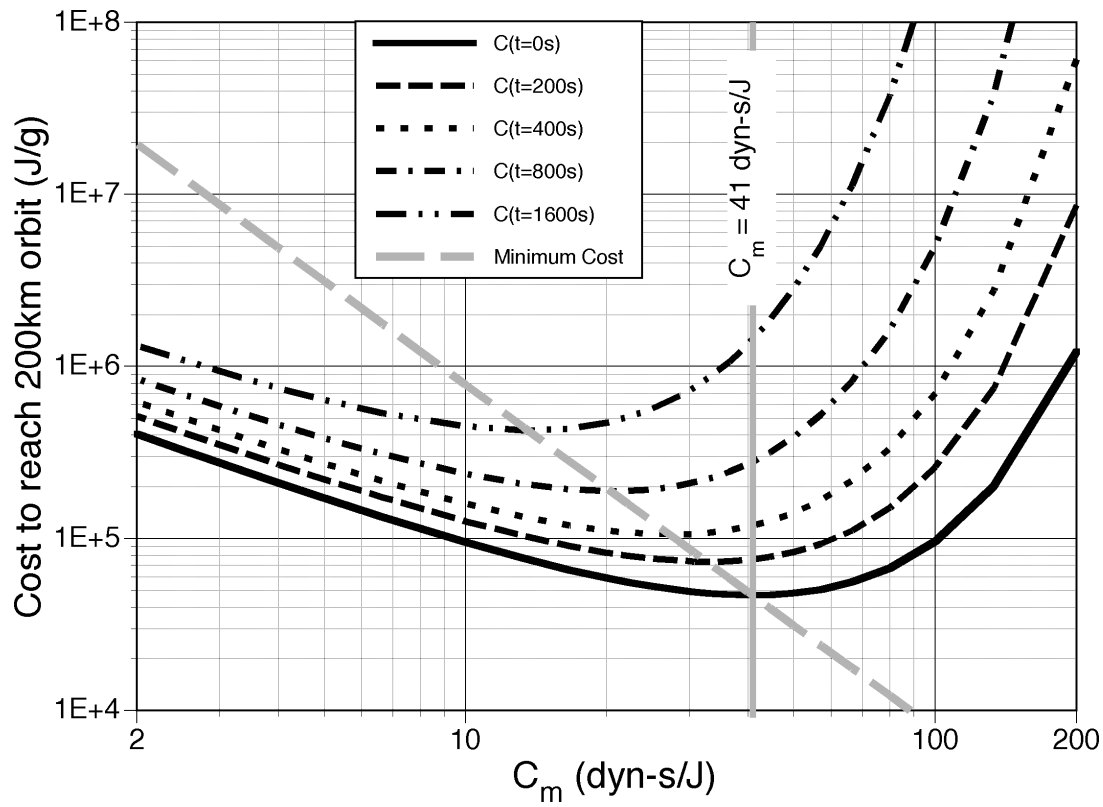


Figure 3. Cost in joules per gram delivered to 200km altitude orbit against gravity, in vacuum for various flight times, as in Figure 1, but versus the maximum coupling coefficient C_m permitted by conservation of energy [$\eta_{AB}=1$].

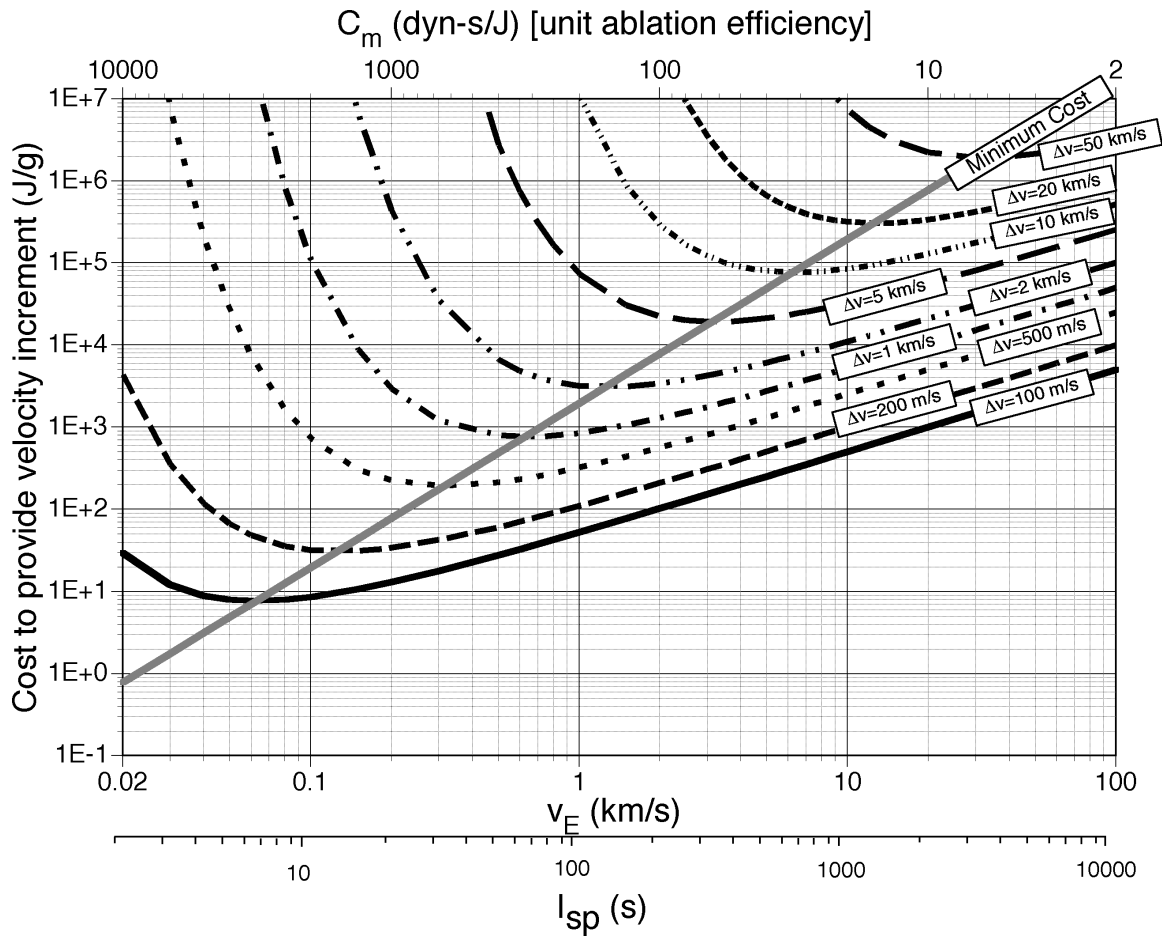


Figure 4. Cost in joules per gram delivered for various magnitudes of velocity increment Δv (vacuum, no gravity). Upper abscissa shows corresponding C_m for unit ablation efficiency, which is the maximum permitted by conservation of energy, given a v_E . This figure illustrates the fact that “giant” C_m values are optimum for missions whose goal is to make small velocity changes. Of course, “giant” C_m values are also useful where the goal is to apply maximum force for minimum laser power, independent of cost. However, lifetime of the ablation fuel is drastically compromised when large C_m is chosen, since $C_m^2 Q^*$ is a constant.

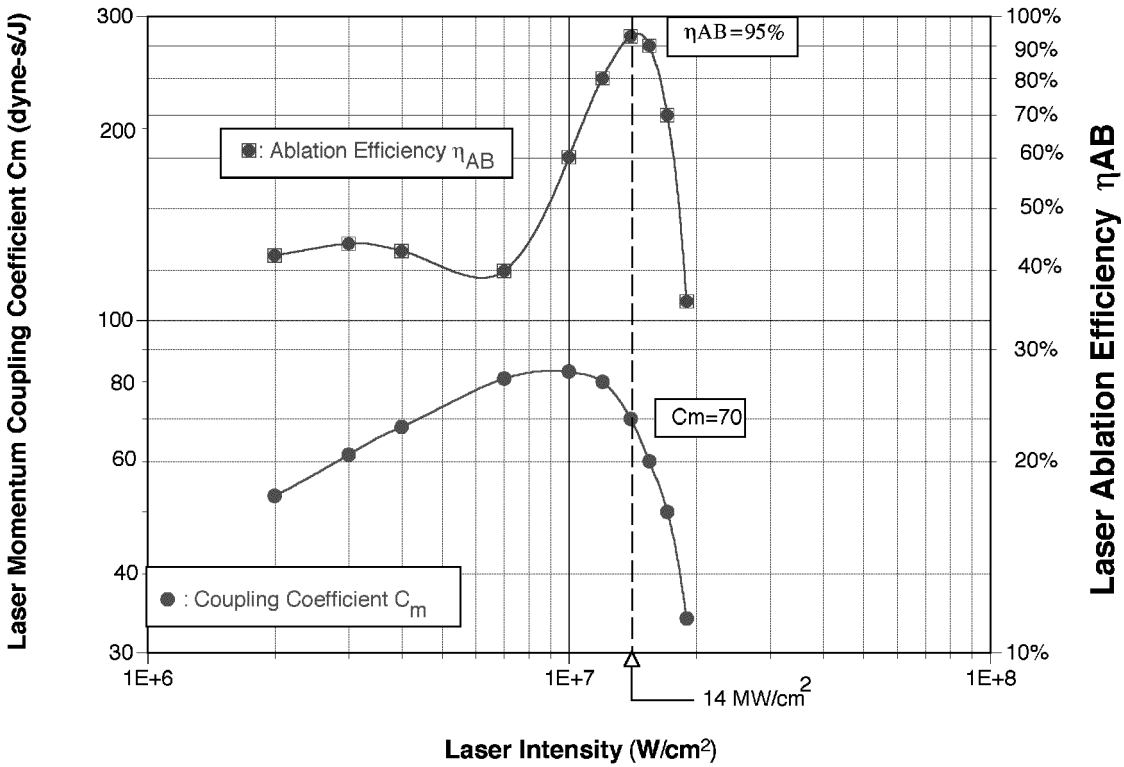


Figure 5. Ablation efficiency can approach 100%, as direct measurements on cellulose nitrate in vacuum [10.6 μm wavelength, 2 s pulse duration] verify. However, the range of parameters for which it does so can be narrow [Phipps and Michaelis 1994]. The impact of $\eta_{AB} < 1$ is that the C_m value deduced from a given v_E may be less than the maximum permitted by conservation of energy.

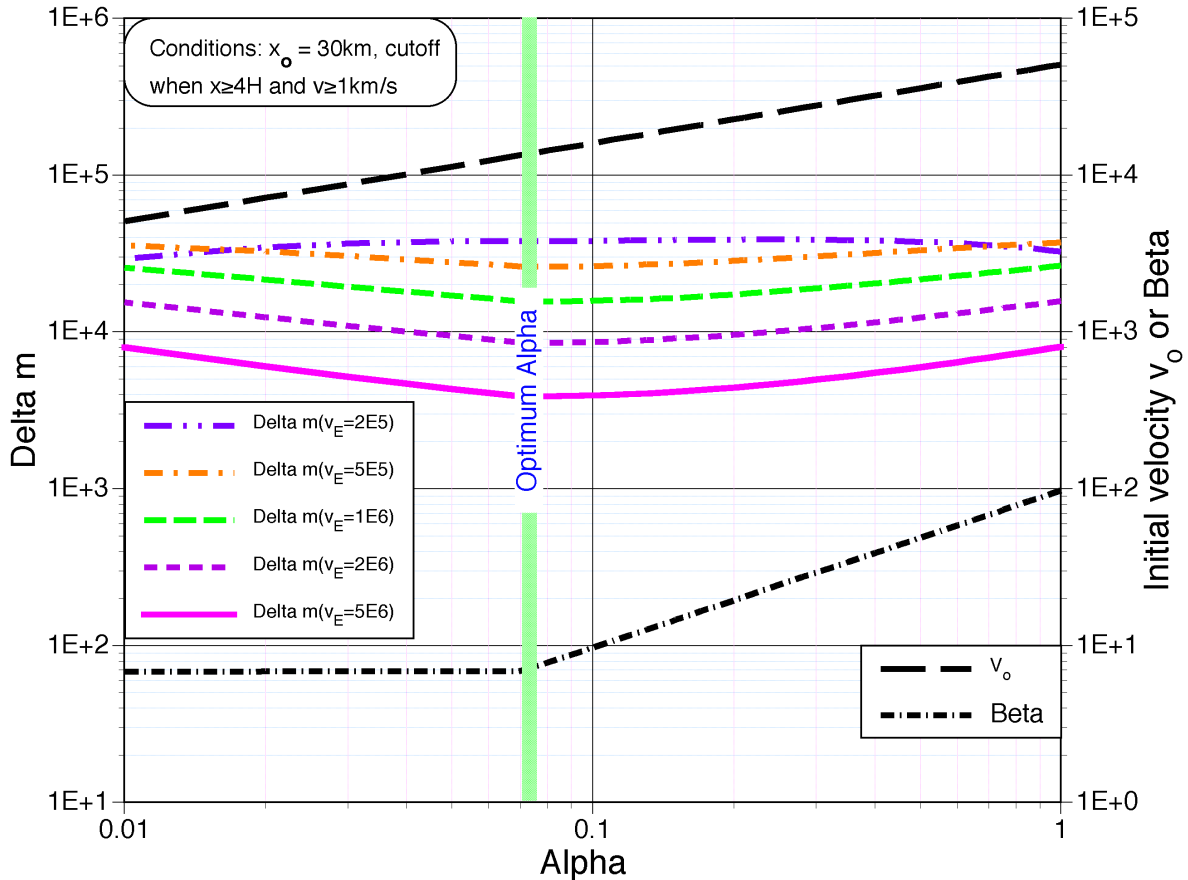


Figure 6. Results of the analysis of optimum parameters for laser driven flights to LEO which begin in the atmosphere. The parameter α is the ratio of drag force in the lower atmosphere to takeoff weight, which determines the velocity profile in the lower atmosphere. Here, initial mass $M=100\text{kg}$ and initial altitude $H_0=30\text{km}$. Exit velocities ranging from $2\text{E}5$ to $5\text{E}6\text{ cm/s}$ are chosen for analysis. Any plot that rises above $\Delta m = 1\text{E}5$ grams corresponds to total exhaustion of the mass M and so represents failure to penetrate the atmosphere. At the optimum α , exit velocity $v_E=5\text{E}5\text{ cm/s}$ works with the expenditure of 30% of the mass M just in penetrating the atmosphere. It is easily seen that $v_E=1\text{E}6\text{ cm/s}$ is much better. These results correspond well to our experience in running simulations with these v_E values. From Table 2, both of the latter velocities require a pulsed laser.

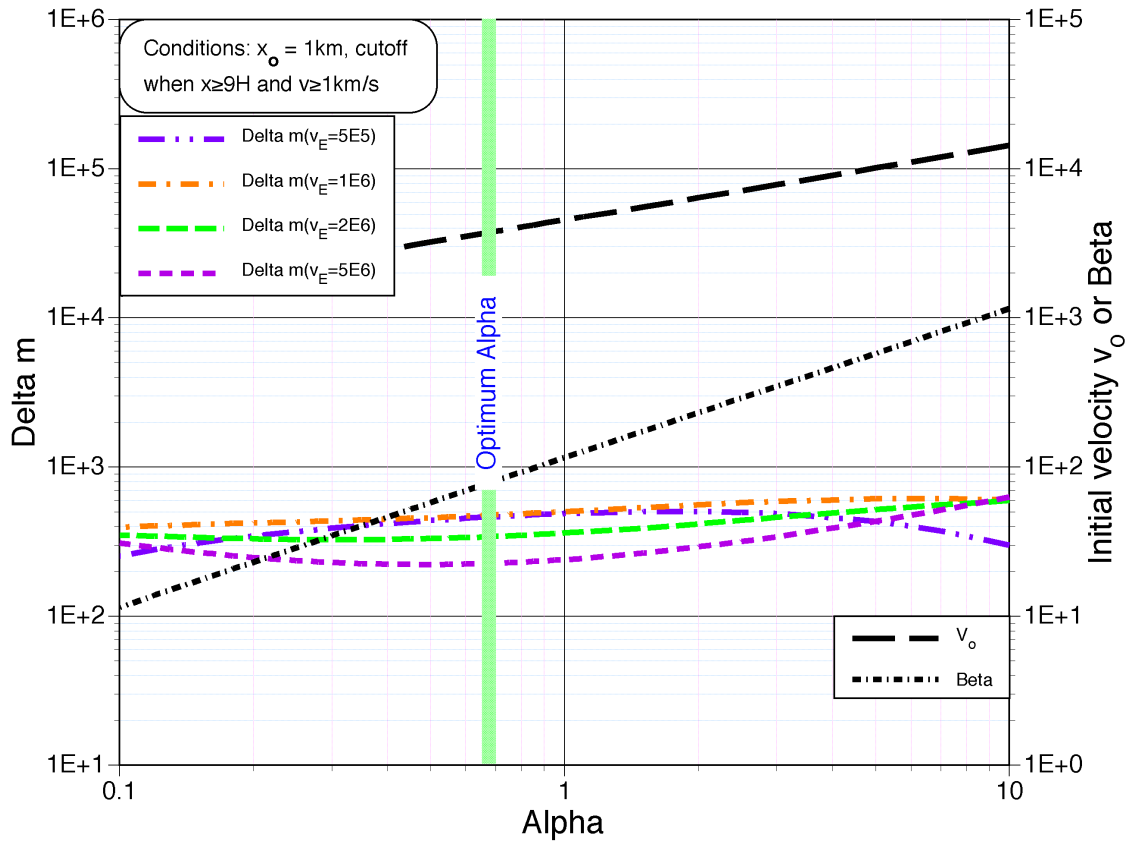


Figure 7. Same as Figure 6, but for laser driven sounding rockets launching from 1km altitude, using several exhaust velocities. Exhaust velocities ranging from 2E5 to 5E6 cm/s are chosen for analysis. Initial mass $M = 1\text{kg}$. Any plot that rises above $\Delta m = 1\text{E}3$ grams corresponds to total exhaustion of the mass M and so represents failure to penetrate the atmosphere. At the optimum $\alpha \approx 0.7$, $v_E = 1\text{E}6 \text{ cm/s}$ works with the expenditure of 50% of the mass M just in penetrating the atmosphere from an initial height 1km. This corresponds very well to our experience in running cases with this v_E . Differences are due to the velocity profiles not being the same as indicated in the model, and to velocity-dependent drag coefficients.

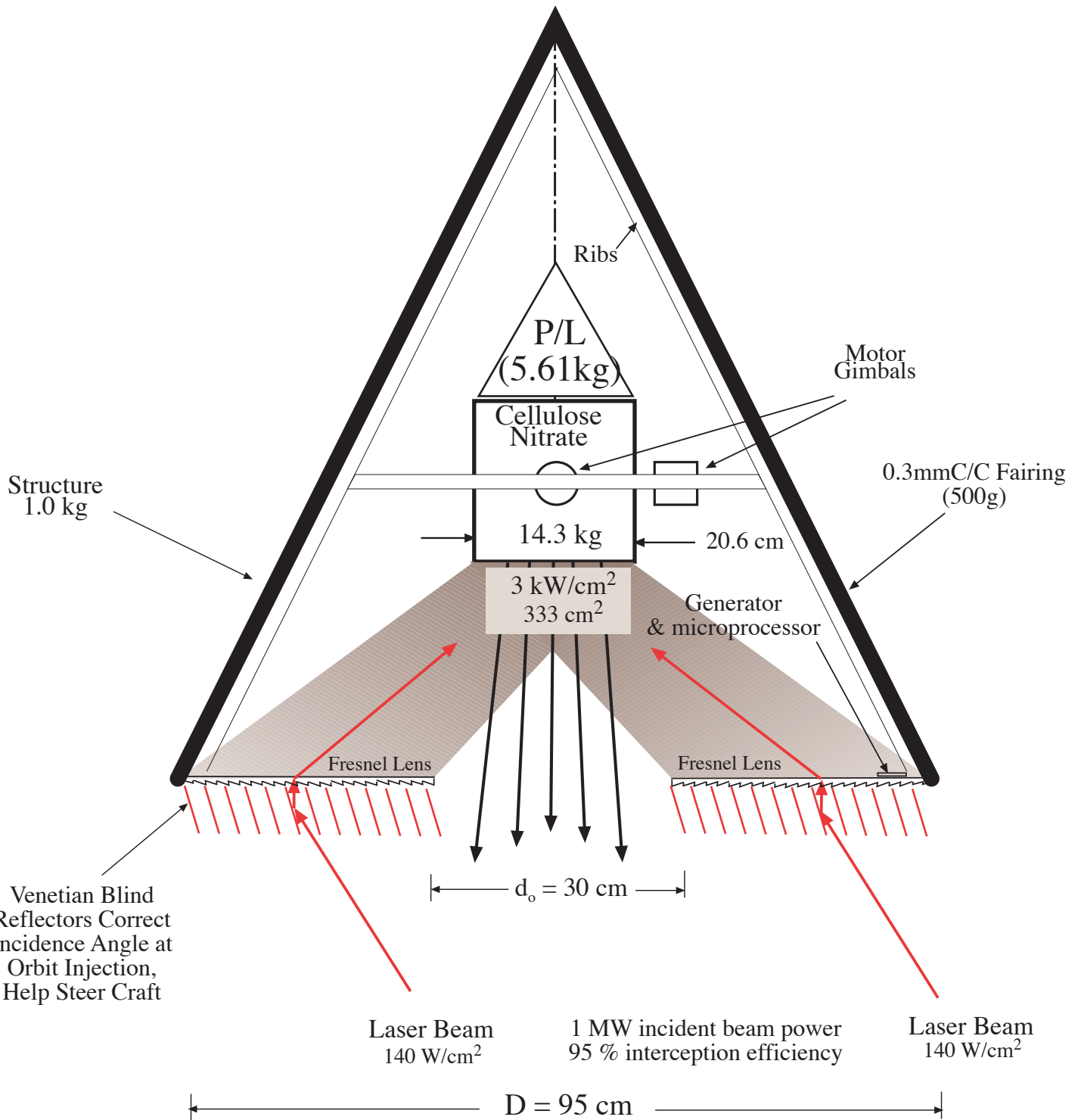


Figure 8. Flyer concept developed for simulations and discussion. Cellulose nitrate has been shown to be capable of large coupling coefficients adequate to match those required in this work [Phipps *et al.* 1990]. A time-average intensity of 3kW/cm² on the ablator is required for the takeoff thrust we assume. In separate work [Reilly, 1996], this figure has also been shown to be adequate for good mechanical coupling by a CW laser. Actively controlled “Venetian blind” reflectors correct incidence angle on the lens during orbit injection, and help steer the craft by altering the illumination distribution so as to bias the temperature across the ablator. Some steering is also provided by the motorized gimbals shown. “P/L” is the true payload, with mass 5.61 kg. Diameter of 95cm is governed by maximum intensity of 140W/cm² on the Fresnel lens with a 1MW laser beam, and diameter-to-length ratio of 1.0 is set by considerations discussed in the text. The carbon composite/carbon fiber fairing is discarded at 120km altitude. Onboard power is provided by a generator which intercepts a small portion of the incident laser beam.

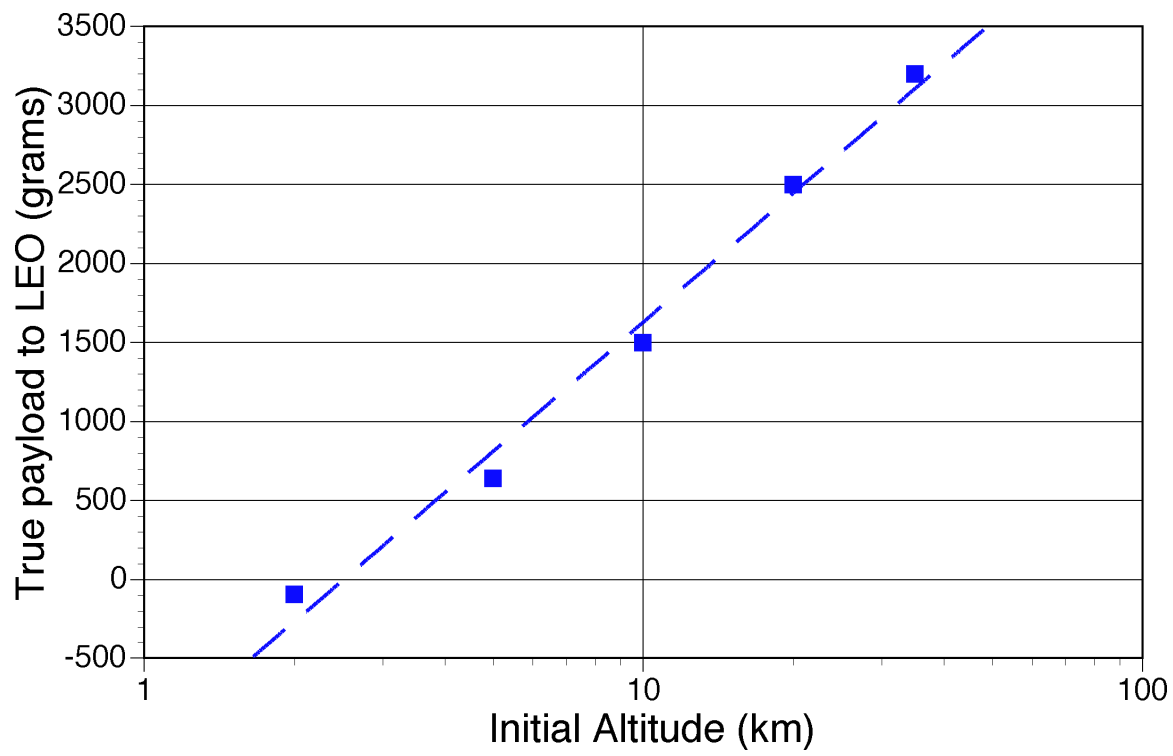


Figure 9. Simulations show dramatic penalties for launching from sea level. In the case shown, laser power $P=1\text{MW}$, initial mass $M=42\text{kg}$, $D=95\text{ cm}$ and $D/L=1$.

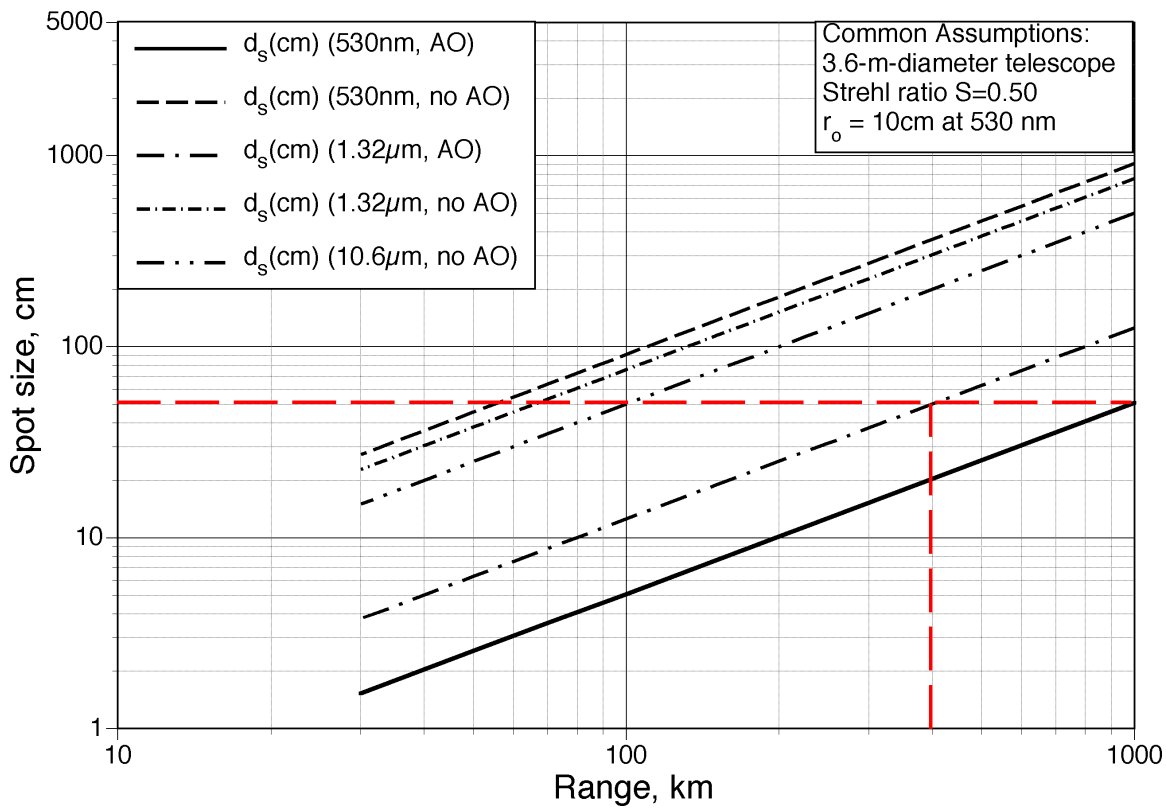


Figure 10. Illumination diameter at the target vs. range for Strehl ratio of 50% (“1.4-times diffraction limited beam”) with a 3.6-meter diameter primary mirror, determined by diffraction at three wavelengths with and without adaptive optics. Telescopes with this size mirror have shown that they can accurately steer at speeds up to 1 /s. At the longer wavelength, no adaptive optics are necessary, because the transverse coherence length parameter r_o is 360 cm, the same size as the mirror. The vertical and horizontal dashed lines indicate that, at a range of 400km, typical for many of our simulations, “spot size” is 50 cm for the iodine wavelength ($\lambda=1.32 \text{ } \mu\text{m}$) with adaptive optics, an acceptable result. However, the CO₂ laser, or the others without adaptive optics, will not provide adequate focusing, even with such a relatively large mirror.

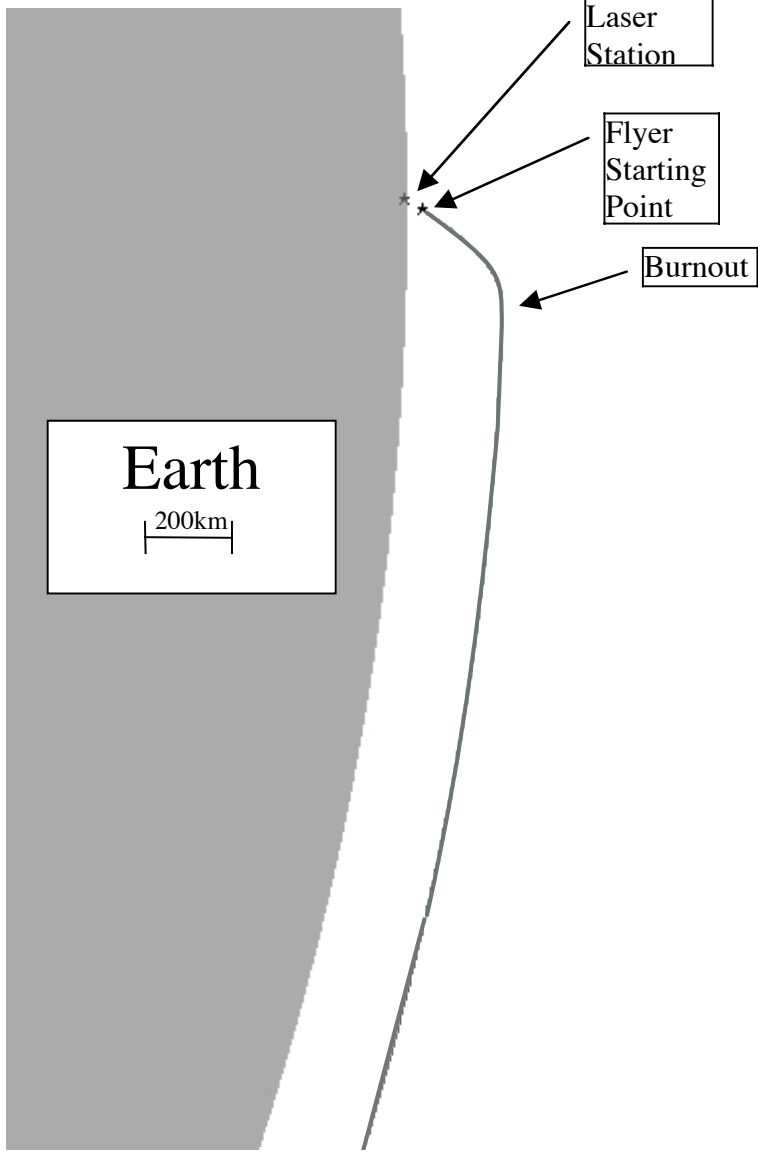


Figure 11A. Trajectory for Light Flyer is characterized by rapid acceleration to orbit and burnout at relatively high elevation angles relative to the laser station.

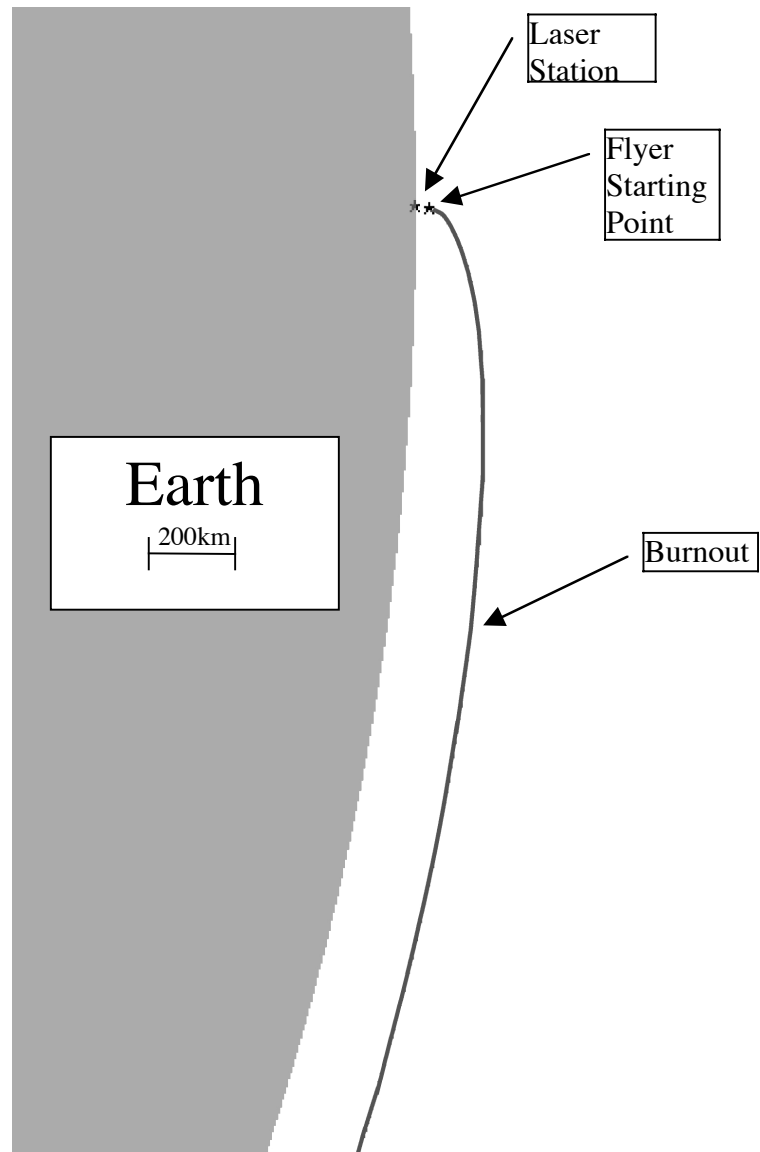


Figure 11B. Trajectory for Heavy Flyer is characterized by slow but efficient acceleration to orbit and burnout at relatively low elevation angles relative to the laser station.

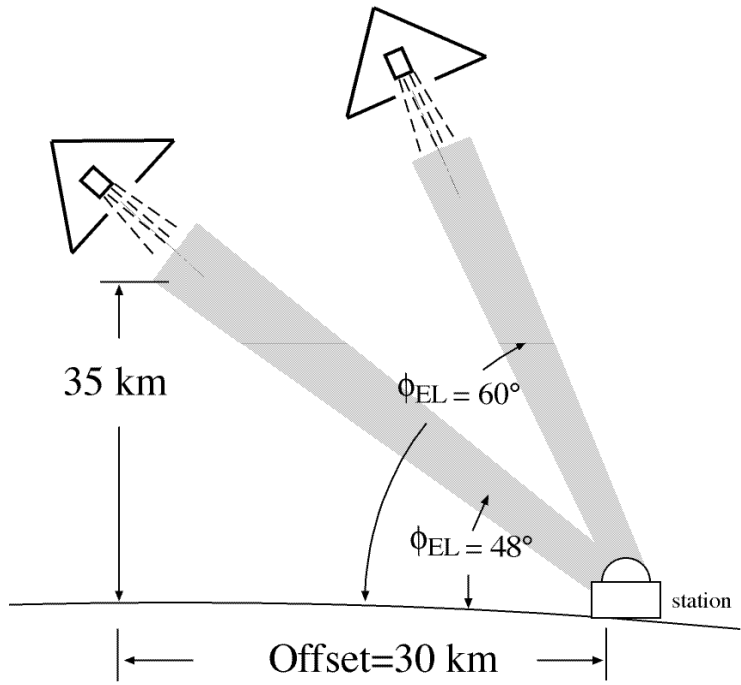


Figure 12A: Attitude of flyer to laser at launch from an elevated platform. Note station offset, which enables flyer illumination incidence angles near zero.

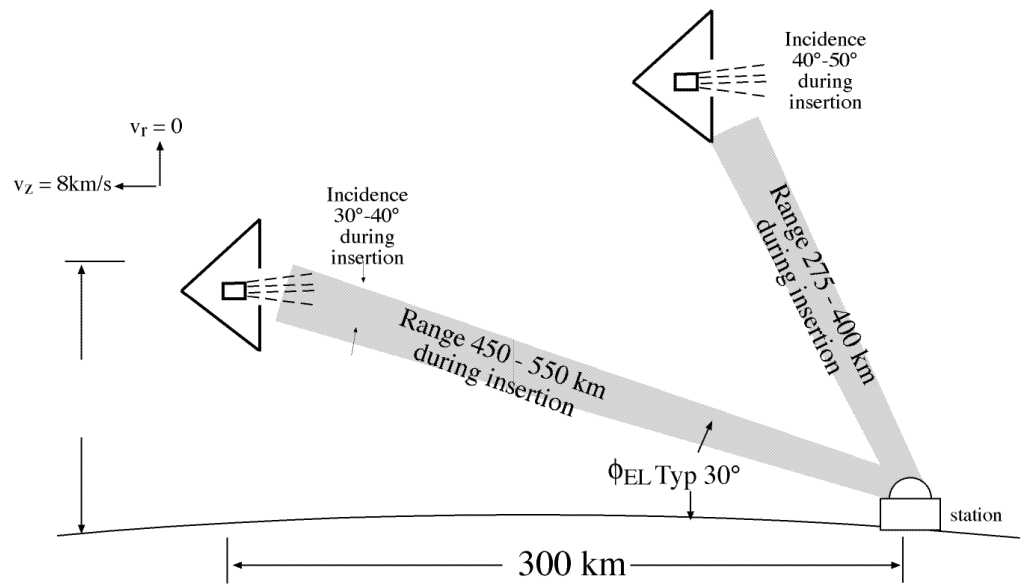


Figure 12B: Attitude of flyer to laser at LEO insertion. Typical dimensions are shown for two different trajectories.

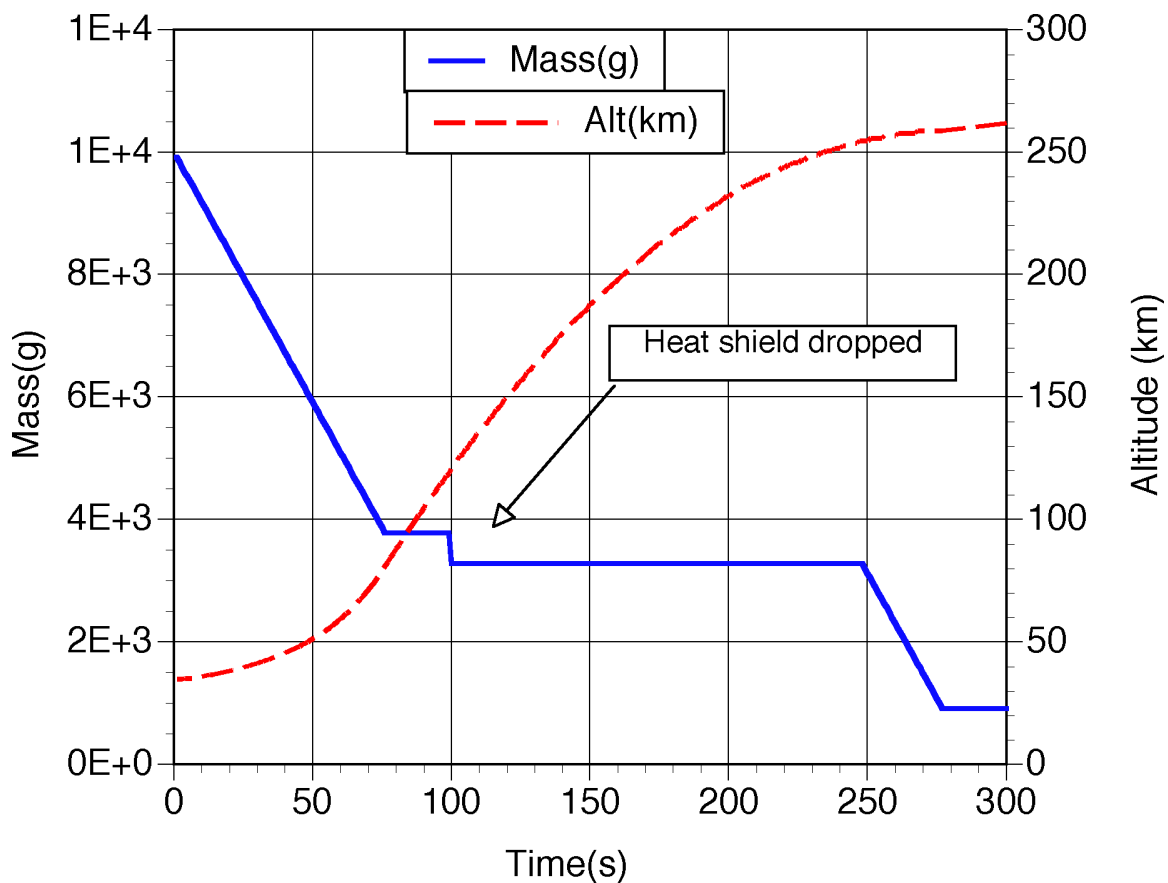


Figure 13. Mass expended during flight 010930. This is a 10kg flyer, launched at 35km altitude (solid line). The heat shield is dropped at 120km altitude. The final orbit injection burn at 250s leaves the flyer at 263km altitude (dashed line).

Flight 071119
 $D/L=1$, $D=95\text{cm}$, $H_0=30\text{km}$, Offset=0, Theta=90°

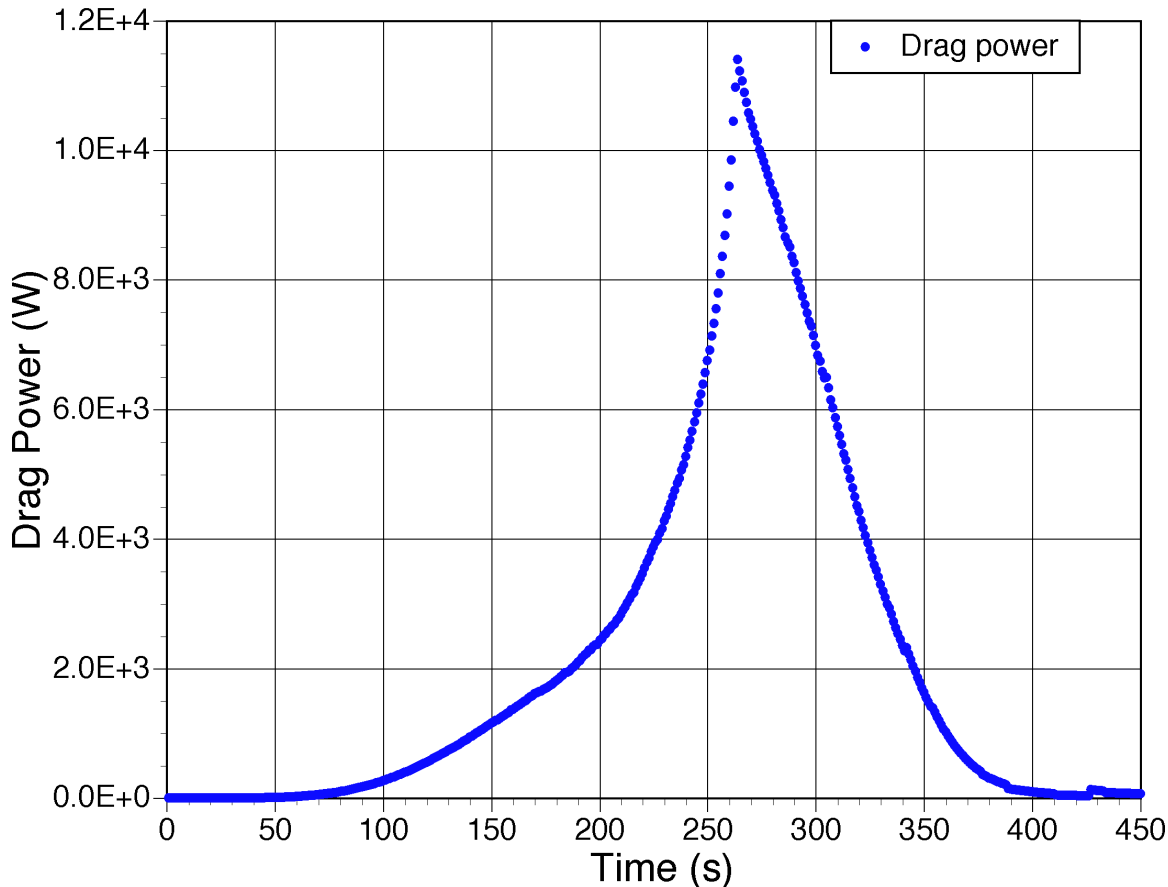


Figure 14. Drag power in the atmosphere can be very reasonable with appropriate speed. Here, the maximum drag power is 11.5kW. Flight 071119 featured initial mass of 20.4kg and delivered mass of 6.1kg [$m/M=0.3$] to a 200-km orbit. Range at burnout was 1300km – a case in which multiple laser stations would be necessary in practice because of Earth curvature.

Flight 121018

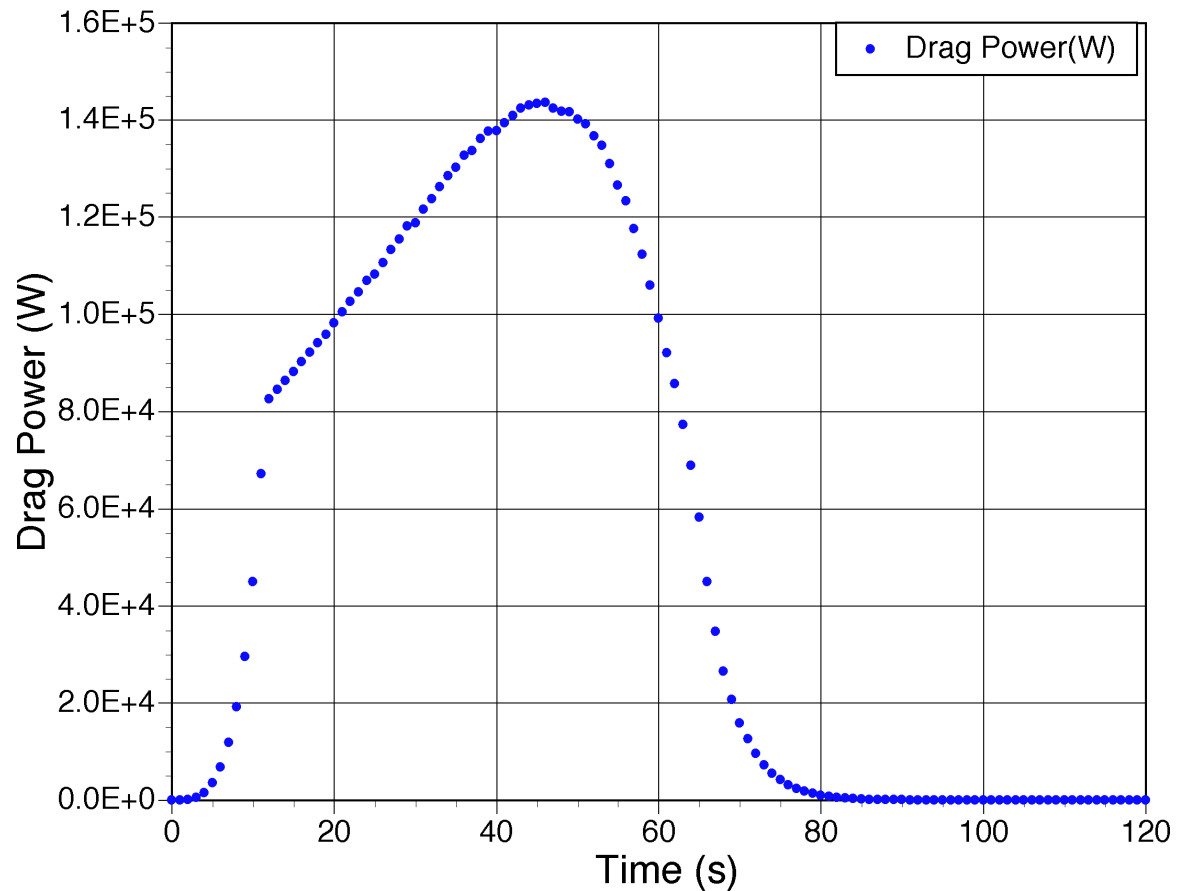


Figure 15. A bad example of drag power profile in the lower atmosphere peaks at 145kW. The resulting m/M was only 0.075.

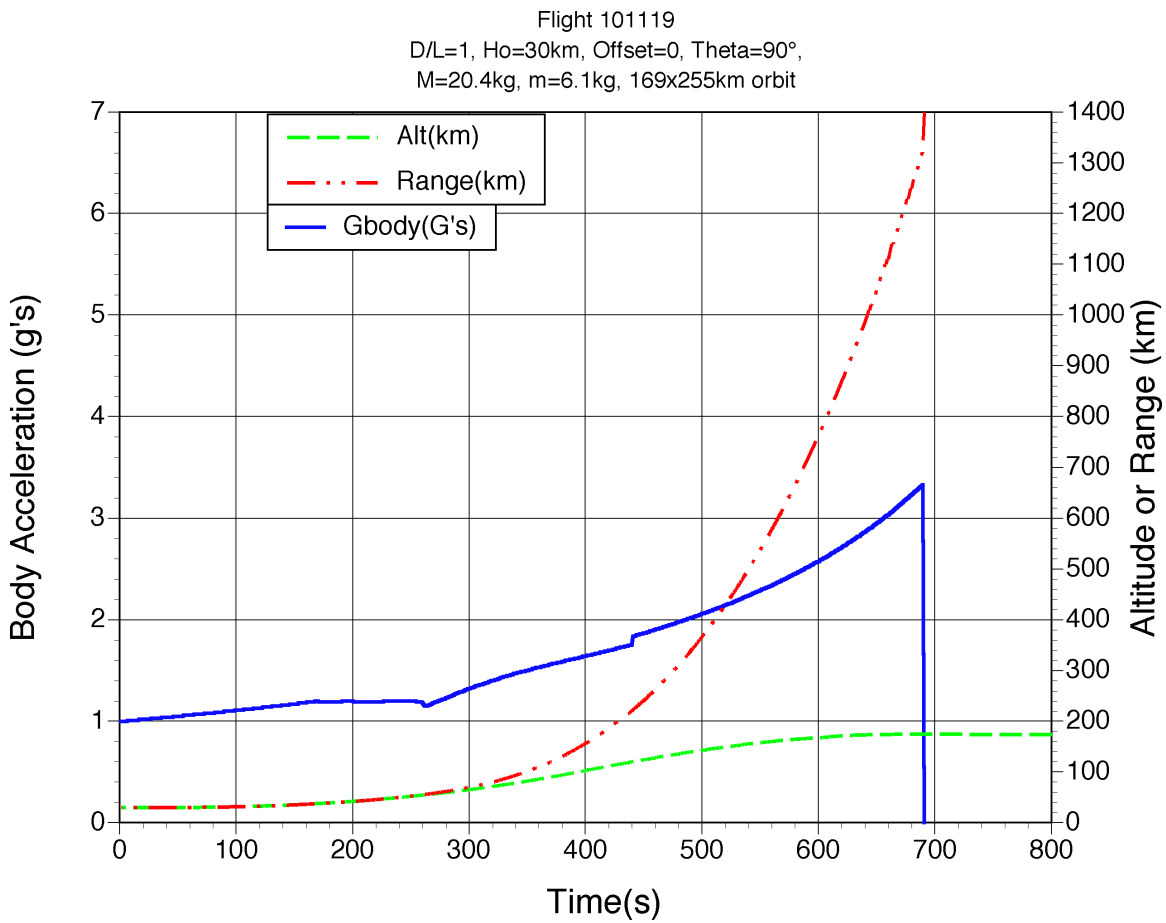


Figure 16A. Illustrative acceleration (solid line), altitude (dashed line) and range profile(dot-dashed line) vs. time for a typical “heavy” flyer. Flight 101119 featured $m/M=0.3$. Blip at 440s in the acceleration comes from dumping the heat shield. Range at burnout is 1380km, and Figure 10 shows that the combination of $\lambda=1.312\text{ m}$ (iodine laser), a 7.2-m diameter telescope and good adaptive optics will handle this range. However, see Figure 17.

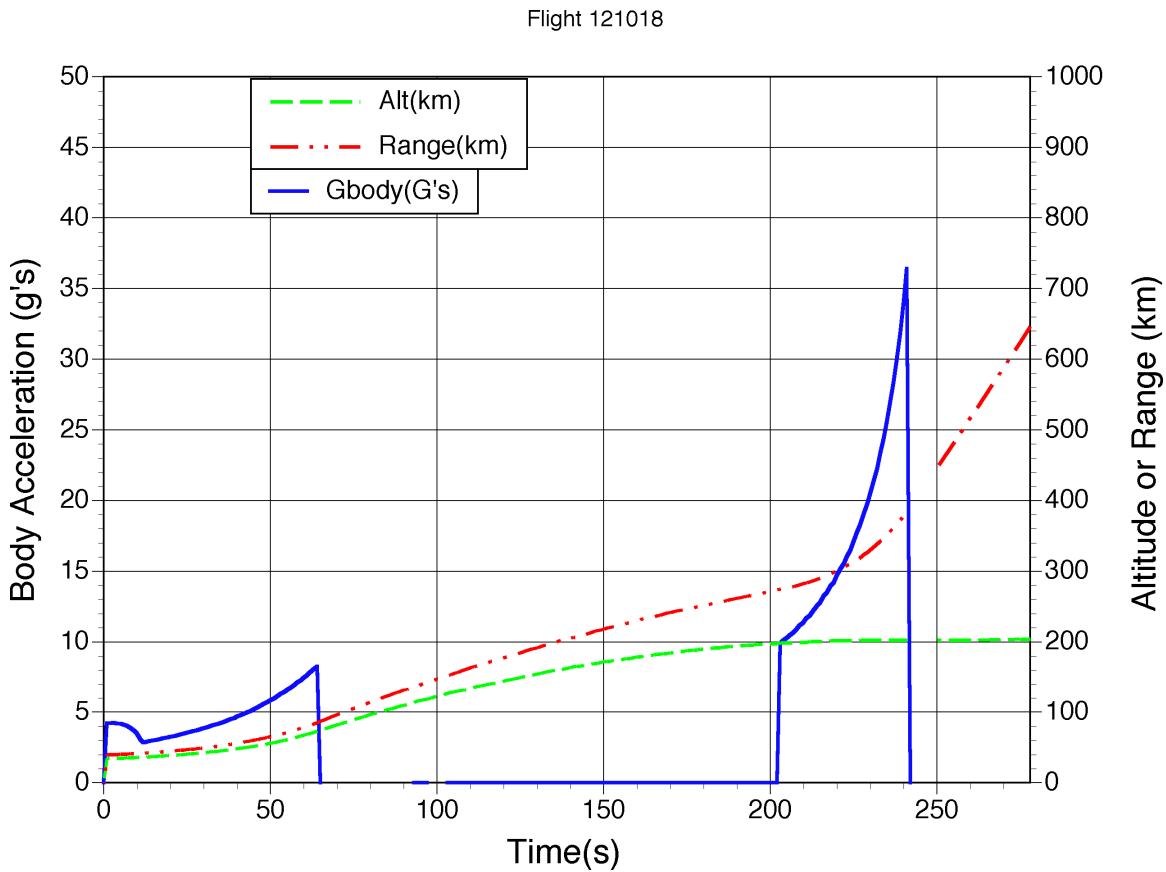


Figure 16B. Illustrative acceleration (solid line), altitude (dashed line) and range profile(dot-dashed line) vs. time for a “light” fast flyer. Fast flyers have a different drive profile than slow ones. After about a 1-minute boost to high velocity, the laser is turned off for over 2 minutes while the flyer coasts up to near-final altitude. Then the flyer is rotated and the laser is turned on for only 40s to produce a final kick to orbital velocity. Flight 121018 featured $M=10\text{kg}$ and a disadvantageous mass ratio $m/M=0.11$, mainly because of high velocity in the lower atmosphere. Maximum acceleration was much higher than in the Figure 16A example, 36G's. Advantages for this flight path were that cutoff range was only 385 km and cutoff elevation angle 30 degrees. Figure 10 shows that the combination of $\lambda=1.312\text{ m}$ (iodine laser), a 1.5-m diameter telescope and good adaptive optics will handle this range.

Flight 101119

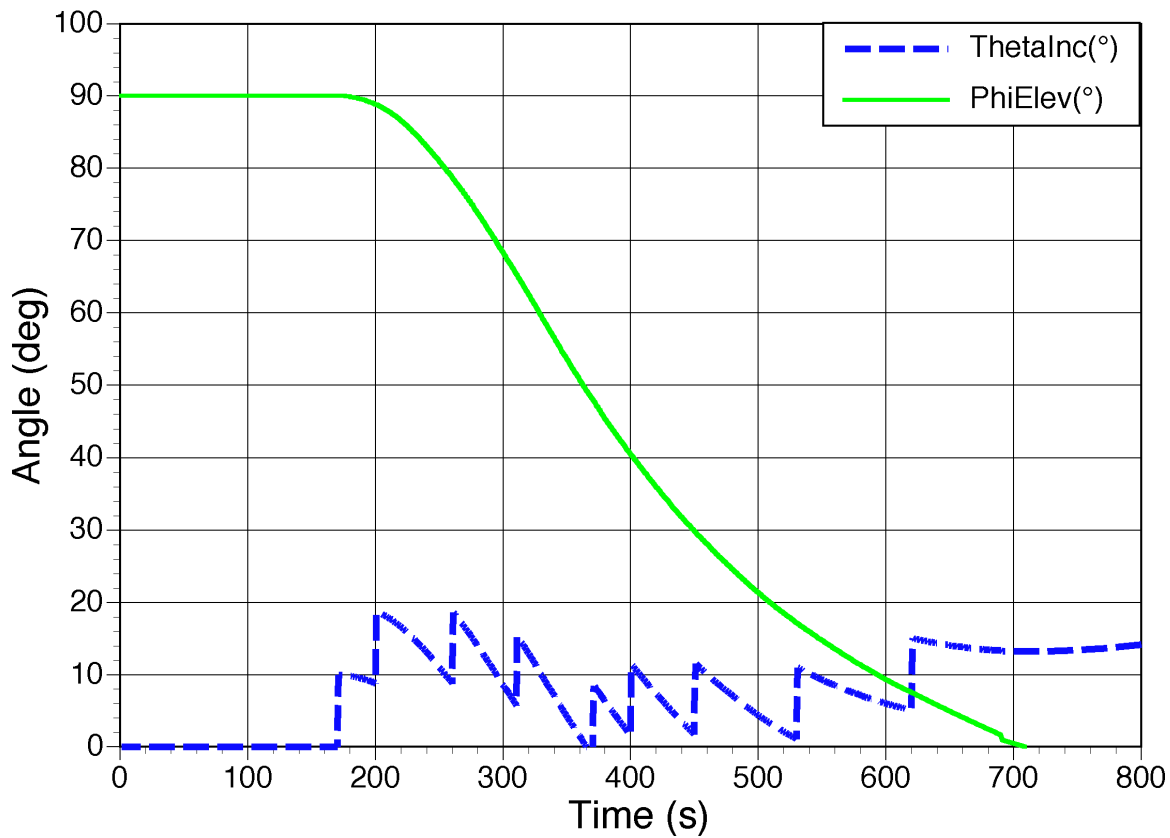


Figure 17. This Figure illustrates that, with a slow “heavy” flyer, it is possible to maintain the angle of incidence sufficiently close to zero throughout a flight as to make the “Venetian blinds” unnecessary. This Figure also illustrates a problem with the otherwise optimum slow flight profile. At cutoff, elevation angle is zero, making beam propagation through the atmosphere to the flyer impossible. Two laser stations distributed along the flight path are necessary.

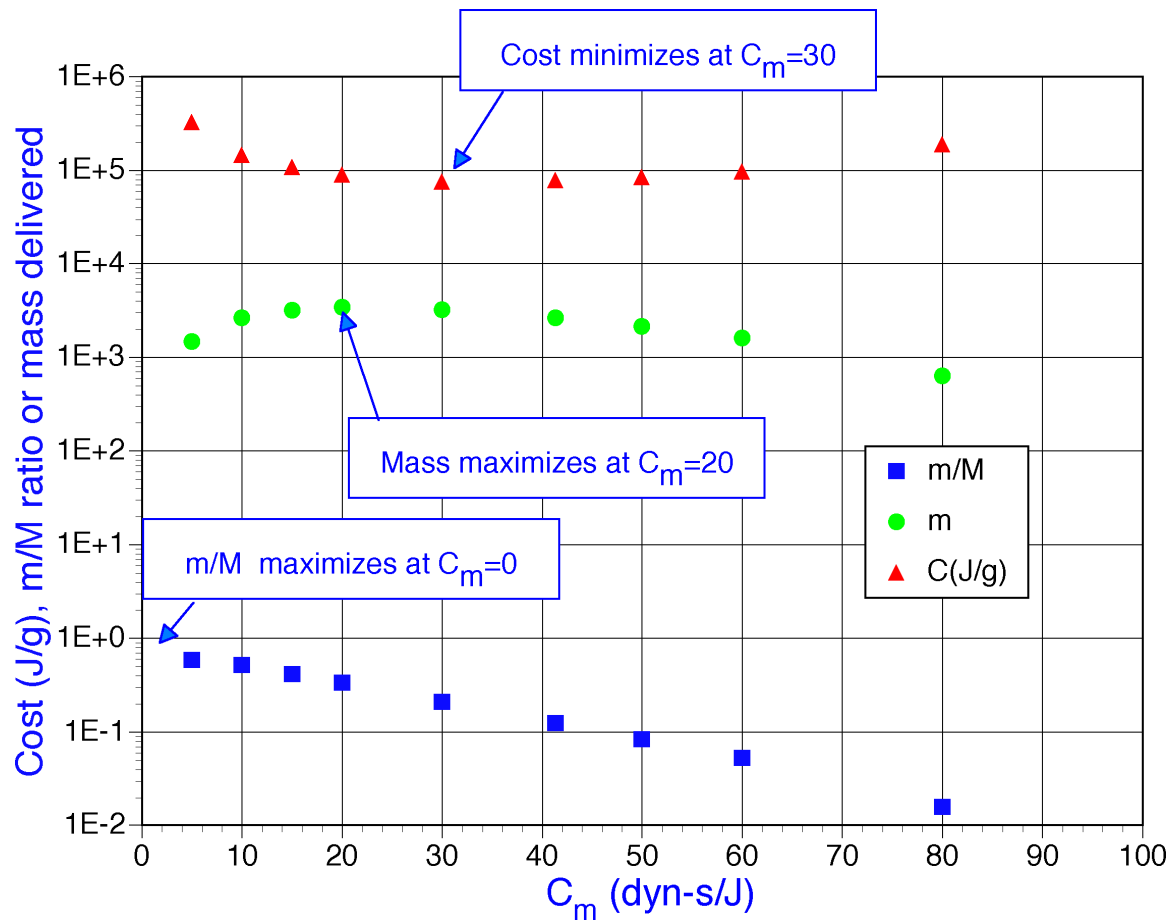


Figure 18. Results of many simulations confirm the analysis, clearly showing that mass, mass ratio and cost optimize at different values of the coupling coefficient C_m . In particular, the mass ratio m/M maximizes at $C_m=0$ [$v_E=\infty$] as theory predicted, the mass delivered to LEO maximizes at $C_m=20$ dyn-s./J [$v_E=1\text{ km/s}$] and cost minimizes at $C_m=30 - 40$ dyn-s/J. Here we assume $\eta_{AB}=1$, so the exit velocity can be obtained as $v_e=2E7/C_m$.

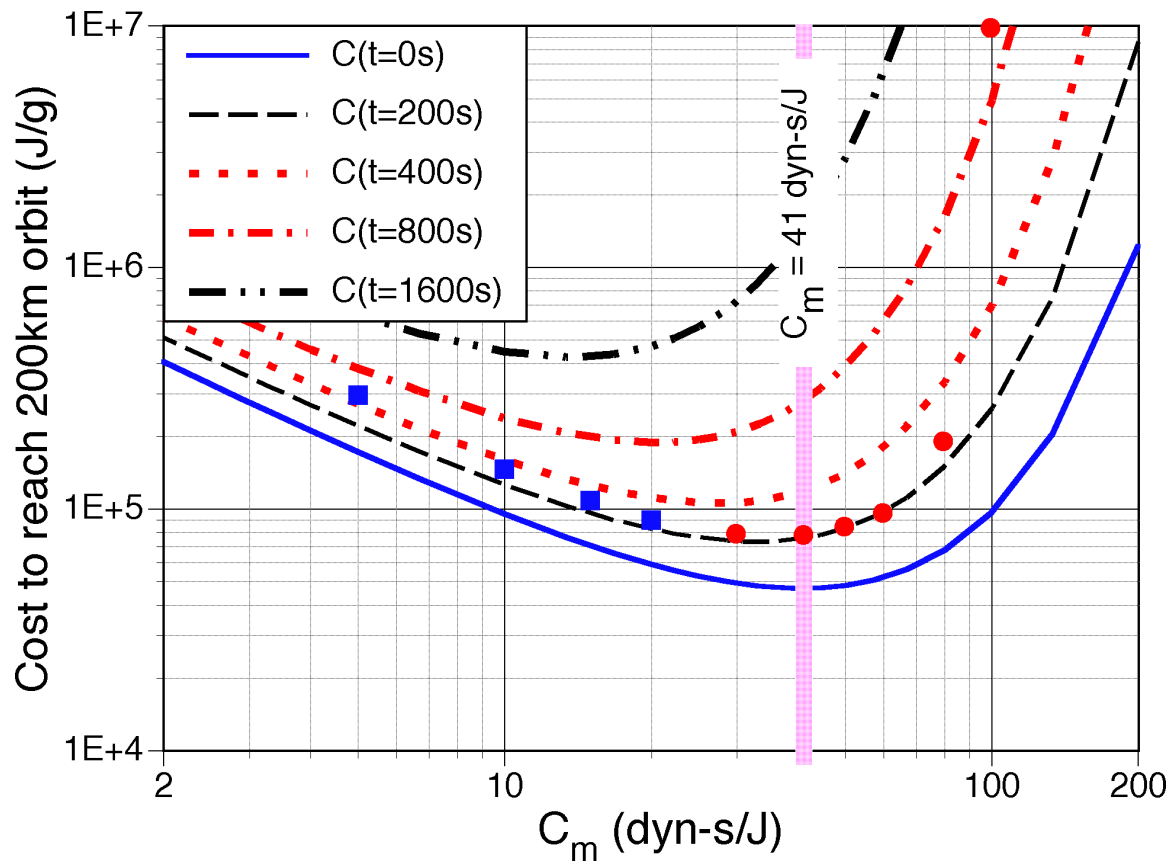


Figure 19. Shows how well optimum simulated flights beginning in the atmosphere at 35 km altitude compare with optimum theoretical cost to orbit in vacuum. Round spots are results for flight times $t \approx 200$ s and square spots are for t approaching 400s because of low C_m . the simulation for $C_m=100$ had infinite cost [zero mass left at end of flight], but is indicated at 10MJ/g. Flights featured 1MW laser power, initial mass M ranging from 2.5 to 51kg to match the C_m chosen, 35 km launch altitude, $D/L=1$ and $D=95$ cm.

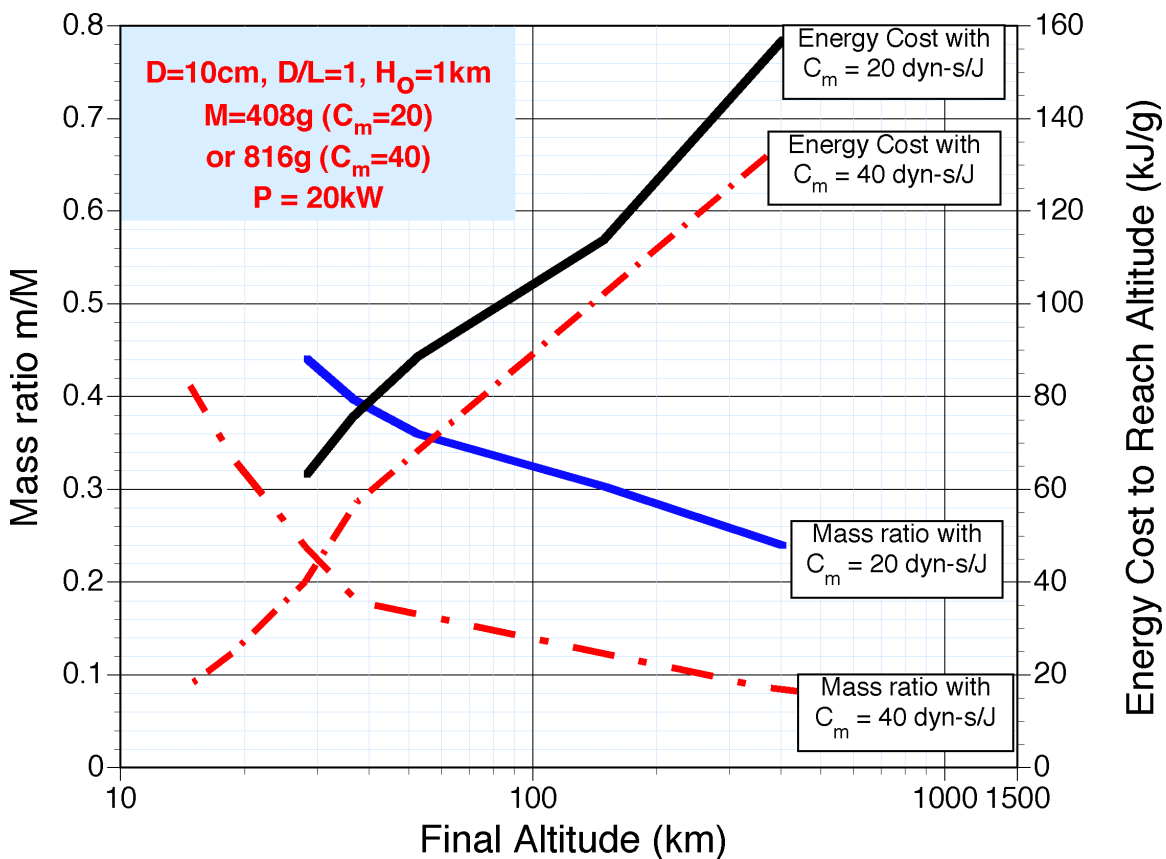


Figure 20. Results of many simulations of 20-kW-laser-driven sounding rocket flights assuming two values of the coupling coefficient C_m , and initial masses which combined with C_m will just lift the flyer initially. Maximum velocity in the lower atmosphere [$x < 30\text{km}$] was maintained at 100-200m/s by starting and stopping the laser. Plotted is energy cost (right ordinate) and delivered mass ratio (left ordinate) vs. final altitude, beginning from 1km elevation. It is seen that mass ratio is better with the lower $C_m = 20$, but cost is lower with $C_m=40 \text{ dyn-s/J}$.

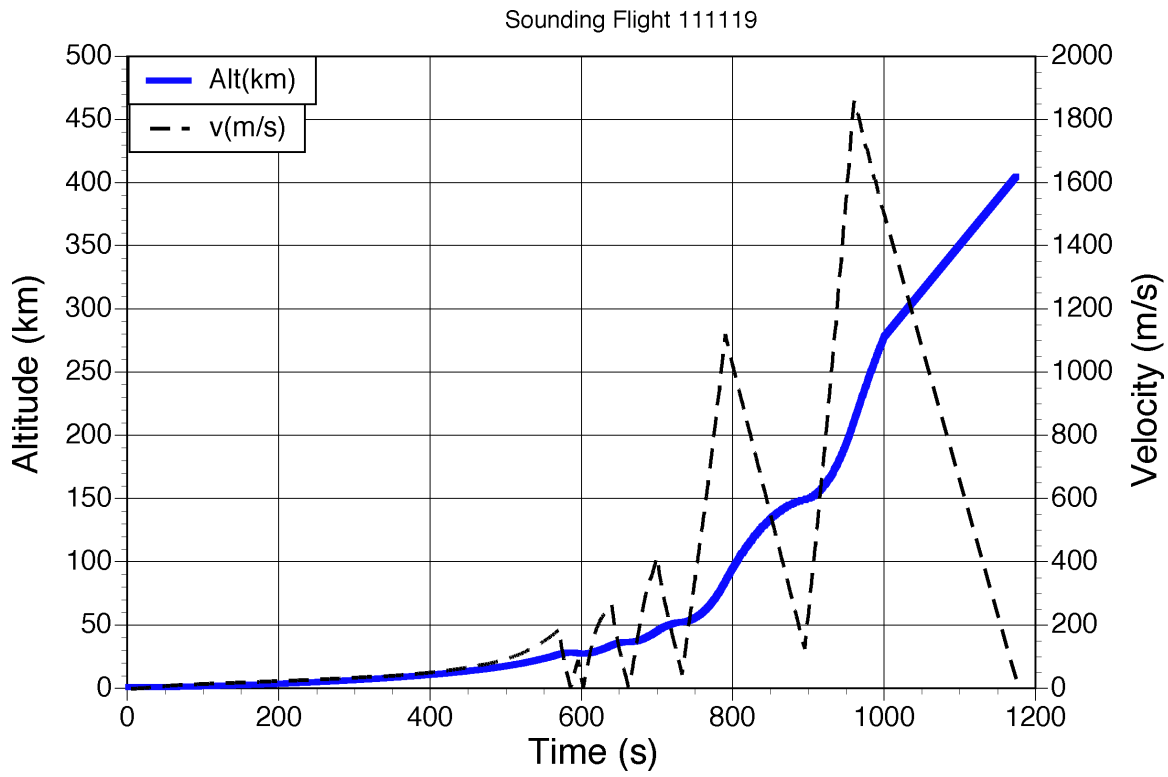


Figure 21. Illustrative velocity profile for a vertical sounding rocket flight, obtained by interrupting laser power to obtain maximum velocity increasing with altitude approximately matching the guidance of section 4 of the text, followed by decay to near-zero velocity. Data in Figure 20 were compiled from conditions at these zeros for several flights.

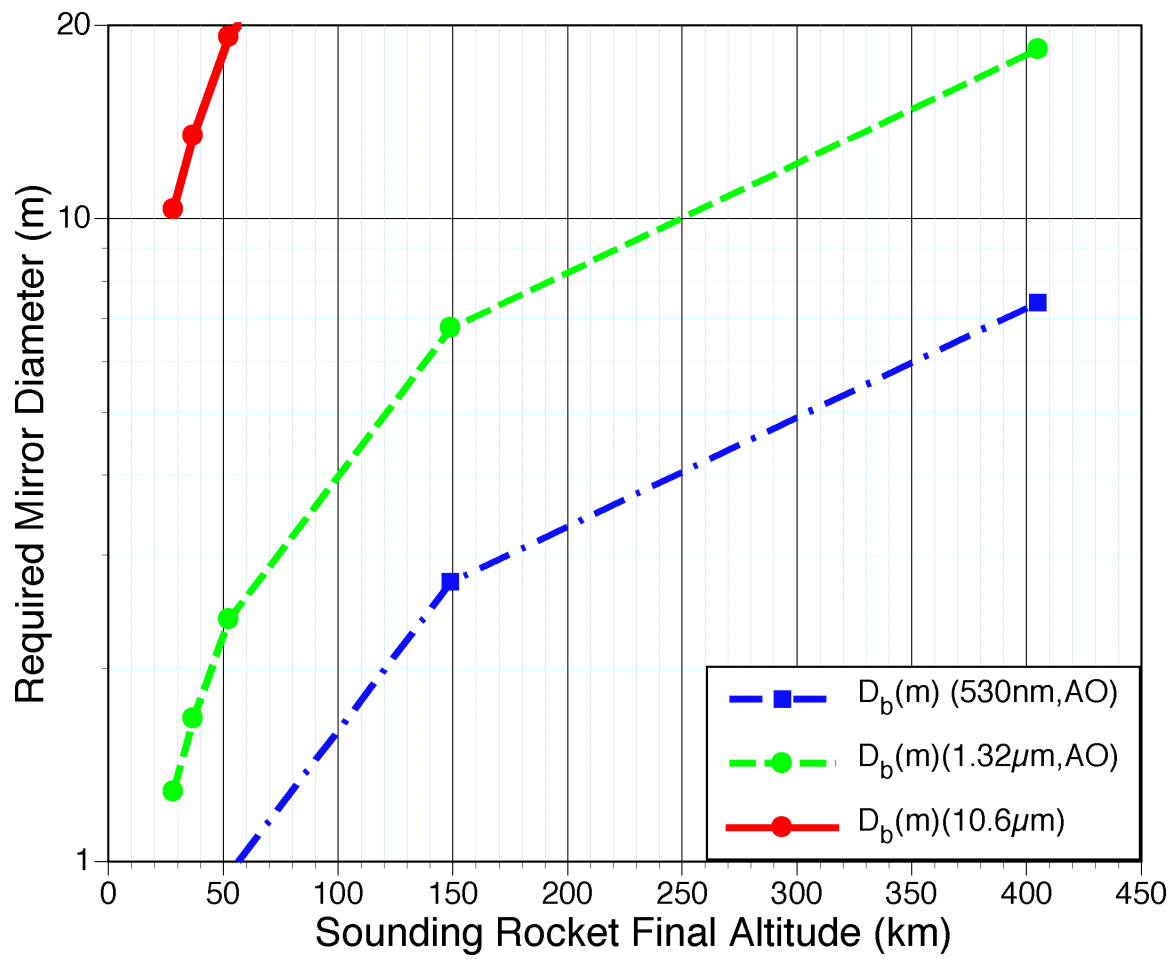


Figure 22. Mirror diameter required to focus on a 10-cm diameter sounding rocket collecting optic at the end of powered flight, for three wavelengths, vs. final altitude achieved by the rocket. Adaptive optics are assumed for the two shorter wavelengths.

Table 1: Present Day Chemical Rocket Launch Costs

Launch System	Minimum Cost (k\$/kg)	Ref.
Rockot	10	Cornara, <i>et al.</i> 1999
Shuttle	18	NASA, 1999; Erskine 1993
Athena 2	16	Cornara, <i>et al.</i> 1999
Taurus	20	Cornara, <i>et al.</i> 1999
Pegasus XL	24	Cornara, <i>et al.</i> 1999
Long March CZ-2C	30	Cornara, <i>et al.</i> 1999
Athena 1	41	Cornara, <i>et al.</i> 1999

Table 2: Maximum laser rocket parameters and intensity I required to sustain them
[$\eta_{AB} = 1$, $\lambda=1.06\mu\text{m}$; $\tau=10 \text{ ns}$ for the pulsed laser]

Given an exhaust velocity, the corresponding ion temperature and specific impulse are given in columns 2 and 3 of the Table. Maximum C_m that could be achieved given the Eq. [4] limit are shown in columns 4 and 5. For the last two rows of the Table, the temperatures are consistent with vapor, not plasma, formation, but these parameters are accessible by CW lasers. The higher intensities are not. For the pulsed laser, T_i is calculated using Eq. [8] of the text.

$V_E(\text{cm/s})$	$T_i(\text{eV})$	$I_{sp}(\text{s})$	$C_m(\text{dyn/W})$	$Q^*(\text{J/g})$	$I(\text{W/cm}^2)$	$\Phi(\text{J/cm}^2)$
5E+6	1.55E+2	5.1E+3	4	1.3E+6	5.2E+11	5.2E+3
2E+6	2.49E+1	2.0E+3	10	2.0E+5	1.3E+10	1.3E+2
1E+6	6.21E+0	1.0E+3	20	5.0E+4	8.4E+8	8.4E+0
7E+5	3.04E+0	7.1E+2	29	2.5E+4	2.0E+8	2.0E+0
5E+5	1.55E+0	5.1E+2	40	1.3E+4	5.2E+7	5.2E-1
2E+5	2.49E-1	2.0E+2	100	2.0E+3	----	----
1E+5	6.21E-2	1.0E+2	200	5.0E+2	----	----

Pulsed Laser
CW

Table 3: Optimum exhaust velocity vs. flight time to reach a 200km LEO orbit.

Flight Time t (s)	V _{eopt} (cm/s)	C _{mopt} [$\eta_{AB}=1$] (dyn-s/J)
0	4.89E5	40.9
200	6.12E5	32.7
400	7.34E5	27.2
800	9.81E5	20.4
1600	1.47E6	13.6

Table 4. Mass Budget for Light Flyer

Seebeck & µprocessor	51 g
Actuators	100 g
Venetian Blinds	80 g
Fresnel Lens	80 g
Heat Shield‡	500 g
Structure	200 g
Ablator Consumed	8.59 kg
Mass to LEO	910 g
True Payload	400 g
Total Mass at Liftoff	10.00 kg

‡ Dumped at 120 km altitude

Table 5. Mass Budget for Heavy Flyer

Seebeck & μprocessor	51 g
Actuators	100 g
Venetian Blinds	80 g
Fresnel Lens	80 g
Heat Shield [‡]	500 g
Structure	200 g
Ablator Consumed	13.78 kg
Mass to LEO	6.12 kg
True Payload	5.61 kg
Total Mass at Liftoff	20.40 kg

[‡] Dumped at 120 km altitude

Table 6. Laser and Flight Parameters for Simulated Flights

Case	Mass-optimized, Fast	Mass-optimized, Slow	Vacuum-optimized, Fast	Vacuum-optimized, Slow
ID#	031209	071119	181210	071020
Mass at Liftoff M	10.0 kg	20.4 kg	21.0 kg	42.1kg
Mass to LEO m	3.20 kg	6.12 kg	2.64 kg	4.92 kg
m/M Ratio	0.32	0.30	0.13	0.12
True Payload	2.69 kg	5.61 kg	2.13 kg	4.41 kg
Flyer Diameter D	95 cm	95 cm	95 cm	95 cm
Diameter-to-Length D/L	1.0	1.0	1.0	1.0
Laser Power	1 MW	1 MW	1 MW	1 MW
C _m	20 dyn-s/J	20 dyn-s/J	41 dyn-s/J	41 dyn-s/J
v _E	10 km/s	10 km/s	5 km/s	5 km/s
Q*	50 kJ/g	50 kJ/g	12.2 kJ/g	12.2 kJ/g
Launch Altitude	35 km	35 km	35 km	35 km
Time to LEO	360 s	690 s	267 s	449 s
Orbit	240x460 km	146x250 km	160x377 km	170x288 km
Initial Acceleration	2.0 G's	1.0 G's	2.0 G's	1.0 G's
Maximum Acceleration	6.4 G's	3.3 G's	15.5 G's	8.4 G's
Peak Drag Power	30 kW @ 55s	11 kW @ 265s	46 kW @ 48s	14 kW @ 175s
T to dissipate radiatively	760 K	590 K	845 K	627
Range at cutoff	720 km	1300 km	473 km	755 km
Elevation angle at cutoff	16 degrees	2 degrees	19 degrees	10 degrees
α_{\max}	0.84 @55s	0.15 @265s	0.69 @38s	0.087@175s
$\langle \alpha \rangle$ 1 st 55s	0.46	0.044	0.31	0.02
Initial β	1.04	0.01	1.0	0.001
Energy Cost C=Pt/m	112 kJ/g	113 kJ/g	100 kJ/g	91.2 kJ/g

Table 7 Proposed Sounding Rocket Test

Laser wavelength	1.315 μm
Laser type	Iodine
Laser power	80 kW
Laser temporal profile	CW ok; pulse better
Ablator diameter	3 cm
Ablator coupling coefficient	20 dyn-s/J
Exhaust velocity	10 km/s
Mirror diameter	3.67 m
Sounding rocket diameter	10 cm
Sounding rocket D/L	1
Ground test site elevation	1 km
Sounding rocket ground mass	408 grams
Sounding rocket ultimate altitude	100 km
Mass delivered to 100 km	98 grams
Approximate flight time	800 s

Appendix I: Symbol Glossary

A	Flyer frontal projected area (cm^2)	M	Flyer initial mass
α	Ratio of drag force to takeoff weight	Δm	The quantity ($M - m$)
β	The ratio $PC_m/(Mg)$ [vacuum case]	M	Mach number, v/c_s
β_a	The ratio $(PC_m - mg)/(mg)$ [atmos. Case]	μ	Exponent of pulse duration in App. IV
b	Mass ablation rate (absolute value)	n	Atmospheric refractive index
C	Energy cost per unit mass delivered (J/g)	P	Laser time-average power
C	Function defined in Eq. [32]	p	Momentum mv
C_d	Drag coefficient	Q^*	Specific ablation energy (a real number) (J/g)
C_m	Impulse coupling coefficient dyne-s/J	R_E	Earth radius
c_s	Sound speed (cm/s)	r_o	Transverse turbulence coherence length
D	Flyer diameter (cm)	r	Earth-centric object orbit radius
D_b	Laser beam diameter at launch (cm)	ρ	Mass density of atmosphere (g/cm^3)
d_o	Size of Fresnel lens opening (cm)	S	Strehl ratio
d_s	Laser beam diameter at target (cm)	τ_{AB}	Ablation fuel lifetime
$\Delta m = M - m$		T_e	Electron temperature
η_{AB}	Ablation efficiency	T_i	Ion temperature
f	Laser repetition rate (s^{-1})	t	Mission time
F	Thrust	t_c	Time at engine cutoff
F	Fluence coefficient in App. V	t_T	Time at turning point
Φ	Target-incident laser fluence (J/cm^2)	τ	Laser pulse duration
ϕ_{EL}	Flyer elevation angle from laser station	τ_{AB}	Ablator lifetime
g	Standard gravity ($980 \text{ cm}/\text{s}^2$)	θ_d	Beam divergence angle due to diffraction
g_R	SRS gain (cm/MW)	θ_{eff}	Effective beam divergence angle
G	Acceleration in Earth-surface gravity units	θ	Flyer zenith angle
Γ	Correction factor discussed in App. V	Δv	Flyer velocity increment (cm/s)
H	Density scale height of the atmosphere	u	Stream speed in App. III; dummy variable in App. V
H_o	Launch altitude of flyer	v	Flyer velocity
h_a	Apogee altitude (cm)	v_E	Effective exhaust velocity (cm/s)
h_p	Perigee altitude (cm)	v_o	Initial speed of flyer
I	Laser intensity on target = Φ/τ (W/cm^2)	v_{rT}	Flyer vertical speed at turning point
I_{sp}	Specific impulse = v_E/g (s)	W	Laser pulse energy
λ	Laser wavelength (cm)	x	Altitude of flyer
L	Flyer length (cm)	x_o	Initial altitude of flyer
L	Angular momentum $mv_\phi r$	ξ	The ratio v_ϕ/v_E in App. V.
m	Flyer mass at time t	z	Range to target (cm)
m_I	flyer mass at orbit insertion	Z	Ionization state of ablation plasma
M_A	Atomic mass number of ablation plasma	ζ	The ratio m_T/m_I in App. V.

Appendix II: Computer Code “DoOrbits”

We developed the code “DoOrbits” specifically to simulate flights of our test shape through the Earth’s atmosphere into Low Earth Orbit. It is written in a compiling Enhanced Basic and tailored for the Power Macintosh® series of computers. With one second virtual steps, an orbit is completed in 120 seconds with $\pm 1\text{km}$ accuracy. On each virtual step, the following operations are performed:

- Update Time
- Get P, C_m, Q*
- Update Impulse
- Get Altitude
- Interpolate Air Density
- Determine if Molecular or Continuum Flow
- Get Temperature
- Get Mach Number
- Get D/L
- Determine Drag Coefficient
- Determine Drag
- Update Geocentric Angle
- Update Slant Range
- Update Elevation Angle
- Update Angle of Incidence on Flyer
- Update Gravity
- Update Vector Acceleration
- Update Vector Velocity & Speed
- UpdatePosition
- Determine Altitude
- Update Mass
- Record New Variable Values
- Check Dialog for:
- Flight profile changes
- Stop command
- Power Off/On command
- Display Off/On command (runs faster off)
- Check for Small-scale to Large-scale plot transition
- Update Plot
- Print every 10th set of key variables to screen

- Check for Automatic Mass or Velocity Cutoff

Menu driven functions are:

Command-S: Save Data file
Command-P: Open PICT file
Command-D: Open Data file
Command-Q: Quit
Command-N: New Calculation
Command-C: Convert Data to EXCEL™ file

Command-R: Open and Replot Data file

Keyboard-driven functions during flight:

Up arrow: Power on
Down arrow: Power off
Tab toggle: Start/Stop screen print
Right arrow: Pause calculation
Left arrow: Decrease thrust elevation angle 10 degrees

Keyboard inputs to initiate a flight are:

Mass at launch
Altitude at launch
Thrust angle at launch
Exhaust velocity
Coupling coefficient
Laser power
Time step
Laser site offset
Cutoff velocity
Heat shield mass (discarded at 120km)
Cutoff mass ratio
Flyer diameter
Flyer D/L ratio

Table A2.1 shows variables which are recorded in the data array.

Operation of Selected Local Functions (subroutines)

1. Atmosphere Density

Density is interpolated between entries of a 90-element lookup table running from sea level to 50,000 km [see Phipps in Campbell, 1996].

2. Molecular Flow

Where M is the Mach number, molecular flow is established when the Reynolds number falls below

$$R = 0.1M \quad . \quad [A2.1]$$

Approximately, we can write

$$\frac{R(x)}{R(0)} = \exp(-x / 6.60) \quad [A2.2]$$

For the variation of Reynolds number with height x (km).

We need sound speed to determine Mach number, not only for the above, but for computing drag. We describe the evolution of sound speed with altitude with adequate accuracy for either purpose in this context by implementing Table A2.2.

3. Drag Coefficient

Drag coefficient has 4 different dependences on parameters, depending on whether flow is sub- or supersonic, and molecular or continuum [Table A2.3].

Table A2.1. DoOrbits Data Array	
index	Variable
0	Remaining mass
1	Time
2	Thrust angle re local horizontal
3	Geocentric angle of radius vector
4	Geocentric radius
5	Downrange distance
6	Radial velocity
7	Downrange velocity
8	Speed
9	Slant range from station
10	Altitude
11	Gravity
12	Body acceleration
13	Power on/off flag
14	Incidence angle of laser beam
15	Elevation angle of flyer from station
16	Drag force
17	Drag coefficient
18	Mach number
19	Molecular flow flag yes/no

These variables are recorded for up to 1000 data points. Prior to cutoff, these are recorded for each time step; after cutoff, each 25th point is recorded. After 1000 points are recorded, the 1000th point will be the last point before Stop.

Table A2.2
Sound Speed vs. Altitude

C_s = (m/s)	From x = (km)	To x = (km)
340	0	0
Ramp to 296	0	11
296	11	34
Ramp to 375	34	50
375	50	60
Ramp to 311	60	80
311	80	∞

Table A2.3 Drag Coefficients for Sub- and Supersonic Speeds, in Continuum and Molecular Flow

Flow⇒ Speed↓	Continuum	Molecular
Subsonic	$C_d = \frac{0.413 (D / L)^{1.18}}{\sqrt{1 + K - M^2}},$ $K = \frac{0.413}{[(D / L)^{0.32} + (D / L)^{0.62}]^2}$	$C_d = [0.4 + 0.6 / M^2] (D / L)^{1.5} + \frac{0.14 (D / L)^{1.8}}{M^{0.8}}$
Supersonic	$C_d = (1 + 4.5 / M)(D / L)$	

Appendix III

Mono-energetic vs. Real Velocity Distributions

In the discussion of laser momentum coupling physics in Section II, a simplifying assumption was made in order to make the relationships among variables more clear. This assumption, stated following Eq. [5], is that the exhaust velocity distribution is to be considered mono-energetic for analytical simplicity. Where by $\langle v_x^m \rangle$ we mean the m-th moment of v_x , this statement allows us to take $\langle v_x^2 \rangle = (\langle v_x \rangle)^2$, a result which would give very misleading results in some circumstances. While it is clear that subsequent mathematics (e.g., Eq. [10a]) will become highly opaque if we carry along the velocity-space integrals which make the analysis rigorous, we need to analyze the error implicit in doing so for a real exhaust stream, to justify the shorthand used in the main body of the paper.

We consider free expansion in the x-direction perpendicular to a planar target of the LISP type. After thermalization has taken place in the stream immediately adjacent to the thin so-called “Knudsen layer” at the laser-heated surface, the velocity distribution of the ablated particles is a full-range three-dimensional Maxwell-Boltzmann velocity distribution with drift velocity u in the x-direction [Kelly and Dreyfus (1988)]:

$$f(v_x, v_y, v_z) = C_x C_y C_z \{ \exp -\beta[(v_x - u)^2 + v_y^2 + v_z^2] \} \quad [A3.1]$$

$$\text{where } \beta = \frac{m_E}{2kT} \quad \text{and } C_i \ni \int_{-\infty}^{+\infty} dv_i f(v_i) = 1. \quad [A3.2]$$

$$\text{That is, } C_x = C_y = C_z = \sqrt{\frac{\beta}{\pi}} \quad [A3.3]$$

In Eq. [A3.2], m_E is the exhaust particle mass. The precise definition of impulse generated by one laser pulse is

$$\delta p = \delta m \langle v_x \rangle \quad [A3.4]$$

$$C_m = \frac{\delta m \langle v_x \rangle}{\Phi}. \quad [A3.5]$$

In the text, we use v_E to denote $\langle v_x \rangle$. With the Eq. [A3.1] velocity distribution,

$$\langle v_x \rangle = \int_{-\infty}^{+\infty} dv_x v_x f(v_x) = C_x [\sqrt{\frac{\pi}{\beta}} u] = u. \quad [A3.6]$$

The amount of kinetic energy in the stream is:

$$e = \frac{1}{2} \delta m \langle v_x^2 \rangle \quad [A3.7]$$

$$\text{where } \langle v_x^2 \rangle = \int_{-\infty}^{+\infty} dv_x \ v_x^2 \ f(v_x) = C_x \left[\frac{\sqrt{\pi}}{2\beta^{3/2}} + \sqrt{\frac{\pi}{\beta}} u^2 \right] = \left[\frac{kT}{m_E} + u^2 \right]. \quad [\text{A3.8}]$$

The ablation efficiency η_{AB} is defined by

$$\eta_{AB} = \frac{e}{10^7 \Phi}. \quad [\text{A3.9}]$$

In the text, we implicitly replace $\langle v_x^2 \rangle$ by $(\langle v_x \rangle)^2$ for analytical convenience. To gauge the consequence of this substitution, we calculate the ratio ψ from Eqs. [A3.4] and [A3.8] and find:

$$\psi = \frac{\langle v_x^2 \rangle}{(\langle v_x \rangle)^2} = \left\{ \frac{u^2 + \frac{kT}{m_E}}{u^2} \right\}. \quad [\text{A3.10}]$$

If, e.g., we take the drift velocity equal to the soundspeed, $u = c_s = \sqrt{\frac{\gamma k T}{m_E}}$, then we find $\psi = \frac{\gamma + 1}{\gamma} = 1.60$.

However, when the angular distribution of particle density in a planar-target laser ablation plume in vacuum is investigated, a preponderance of measurements summarized in Kelly and Dreyfus (1988) and in Phipps and Dreyfus (1993) show forward peaking which is highly pronounced relative to the angular distribution predicted by Eq. [A1] with a sonic drift velocity $u = c_s$. Where θ is the angle to the surface normal, it is observed that the detected plume distribution varies like $\cos^\nu \theta$, with several experiments giving a beam-like expansion with $\nu = 8 - 10$.

This beamlike behavior of real ablation jets, in which the halfwidth at half-maximum is of order 20 degrees, is the reason why we need not consider anything more complex than ablation from planar targets in this work. Nature forms the jet already.

Kelly and Dreyfus show that, introducing the drift velocity Mach number $M = u/c_s$, $M = 1$ should correspond to $\nu = 4$, whereas $\nu = 8 - 10$ corresponds to $M \approx 2$.

In other words, the flow in high-intensity laser ablation is supersonic. This rather strange result has two causes whose relative importance has not yet been assessed. These are 1) acceleration of the stream due to unsteady adiabatic expansion beyond the Knudsen layer as discussed by Kelly and Dreyfus (1988) and 2) electrostatic acceleration of the ions in the plasma stream by the collisionally-decoupled high-energy tail of the electron velocity distribution as discussed by Phipps and Dreyfus (1993).

$$\text{When } M = 2, \quad \psi = \frac{4\gamma + 1}{4\gamma} = 1.15 \quad [\text{A3.11}]$$

In the above we have taken the specific heat ratio $\gamma = c_p/c_v = 5/3$ (the ideal gas value) which is valid for the typical laser space propulsion plume.

In fact, the assumptions made in writing Eqs. [3 – 5] of the text are fairly good. Further, it is important to note that

$$\eta_{AB} = \frac{\delta m \langle v_E^2 \rangle}{2 \times 10^7 \Phi} \geq \frac{\delta m \langle v_E \rangle^2}{2 \times 10^7 \Phi} \quad \text{overestimates } \eta_{AB}.$$

Appendix IV: Pulsed Laser Requirements on Target and in the Atmosphere

In the main text, we indicated that repetitively-pulsed lasers have certain advantages over CW lasers for reaching the temperatures required for efficient ablation exhaust velocities, but did not describe in detail how the intensities required can be calculated, or how these affect laser propagation in the atmosphere. This description is the purpose of this Appendix.

Fluence Required on Ablator to Achieve Optimum Coupling

As incident pulsed laser fluence increases past threshold, the momentum coupling coefficient C_m rises rapidly to a peak value [Figure A4.1], declining slowly for further increases in fluence. The sharply rising side of this curve is due to the vapor-plasma transition. The decline is due to two factors: a) C_m is defined in such a way ($C_m \propto \Delta m v_E / \Delta m v_E^2$) that it behaves like $1/v_E$ above the intensity sufficient to cause most of the laser pulse energy to couple into the exhaust plume rather than the substrate and b) the nearly simultaneous onset of plasma shielding of the substrate.

Figure 5 of the text shows it is not necessary for maximum C_m values at Φ_{opt} to be limited to the 5 – 10 range.

In order to determine what fluence is required to achieve optimum coupling on the ablator, we surveyed the results of 50 experiments in which this optimum fluence Φ_{opt} was measured or could be deduced, and determined that for a wide variety of possible debris surfaces, wavelengths ranging from 0.25 to 10.6 μm , and pulselengths $1\text{ps} < \tau < 1\text{ms}$, data for Φ_{opt} can be best fit by a trend:

$$\Phi_{opt} = F \tau^\mu \quad \text{J/cm}^2 \quad [\text{A4.1}]$$

with $\mu = 0.41 - 0.45$ and $F = 1.5E4 - 2.3E4$ depending on whether or not the ps-pulse points are included in the fit (see Figure A4.2). Thermal transient theory would give $\mu = 0.5$ for this exponent. Alternatively, in terms of beam intensity on target,

$$I_{opt} = F \tau^{\mu-1} \quad \text{W/cm}^2 \quad [\text{A4.2}]$$

While vastly different physics governs the detailed absorption and ionization processes which occur over this range of parameters and materials, the plot permits us to estimate the fluence which must be delivered to an ablator within the accuracy required to assess SRS in the atmosphere, for example, or whether lasers with the required pulse energy are feasible.

Our purpose is to determine the beam intensity I_b which we can propagate through the atmosphere at a given pulselength and wavelength and reach the flyer's collecting optic (not the ablator itself) with an appropriate spot size. Since many nonlinear effects in the atmosphere scale as $1/\lambda$, it is convenient to plot I_b/λ , rather than I_b , vs pulselength,

so that trends for different λ will nearly superpose in a graphical representation of these limits.

We computed nonlinear process limits using standard references, integrating up through the atmosphere in several zones of varying density and temperature. [For Stimulated Raman Scattering, see: Carman, *et al.* 1970; Fulghum *et al.* 1984; Heeman, *et al.* 1995; Henesian, *et al.* 1985; Herring, *et al.* 1986; Ori, *et al.* 1990; and Pennington, *et al.* 1988. For nonlinear index of the atmosphere, see: Carman, *et al.* 1988; Hellwarth, R. W. 1995; Hellwarth, R. W. 1975 ; Hellwarth 1990; Marburger, 1975; Phipps, *et al.*; Shaw, *et al.* 1990 and Wolfe and Zyssis].

For the near field (close to the laser transmitter), Figure A4.3 shows the resulting nonlinear process limits in the Earth's atmosphere, leaving a free operating region below these limits where pulsed beams going from Earth to space can operate. This Figure is an update of Figure 17 of Phipps, *et al.* 1996.

It can be seen that SRS is the primary limit for collimated pulses of duration $300\text{ps} < \tau < 10\mu\text{s}$, while, for shorter pulses, nonlinear index is the main limit. STRS (Barnard 1989) – a microscopic analog to whole beam thermal blooming which creates thermal gratings that scatter the beam – becomes dominant when pulse duration exceeds $10\mu\text{s}$. For our purposes in launching laser ablation rockets, this leaves a lot of room for operations. The example shown in Figure A4.3 avoids all the limits in a collimated (unfocused) beam while permitting the propagation of 10-kJ single pulses at 100ns, or 100-kJ pulses at $10\mu\text{s}$, from modest-size apertures. A repetition rate of 100Hz or 10Hz, respectively would create 1MW average power, even with such a small beam.

In the Lightcraft case, particularly just after launch, however, the beam is focused, not collimated. At short range, the pathlength is small in the product gRI_bz , but intensity is much larger, averaging through the beam, over the short path than it was at the launching telescope. SRS gain is essentially constant over the first 40km of atmosphere [Figure A4.4] and then drops rapidly to zero. To obtain useful pulse fluence limits for launching a Lightcraft, we need to integrate through the atmosphere for a cone-shaped converging beam as flyer range varies [Figure A4.5] to be sure the limits are not exceeded for any range, and to compare wavelengths. To add to the complexity, single pulse energy in the beam (column 3, Table A4.1) must be set equal to that amount which, when focused by a 95-cm-diameter collecting optic onto a 20.6-cm diameter ablator (as in Figure 8), Eq. [A4.2] will just be satisfied.

We did this, and the results are shown in Figure A4.6 and in Table A4.1. The short summary is that the “safety factor” disappears at 530nm with the parameters chosen, whereas, at $11.1\mu\text{m}$, it is very comfortable. This is because we deliberately chose mirror sizes to highlight the difficulties of avoiding SRS in a focusing situation early in the flight, while delivering the intensity to the flyer's collector optic required to get optimum coupling on the ablator. The telescope diameter for the two shorter wavelengths is governed by achieving this safety factor rather than by letting mirror diameter be as small as it could be if governed by diffraction.

Note that, if we used the same mirror size at $1\mu\text{s}$ pulselength, SRS limits would be exceeded [Table A4.1] and this fact shows why we have picked 100ns for the pulselength in our discussions.

These features were not apparent from the analysis for a collimated beam [Figure A4.3].

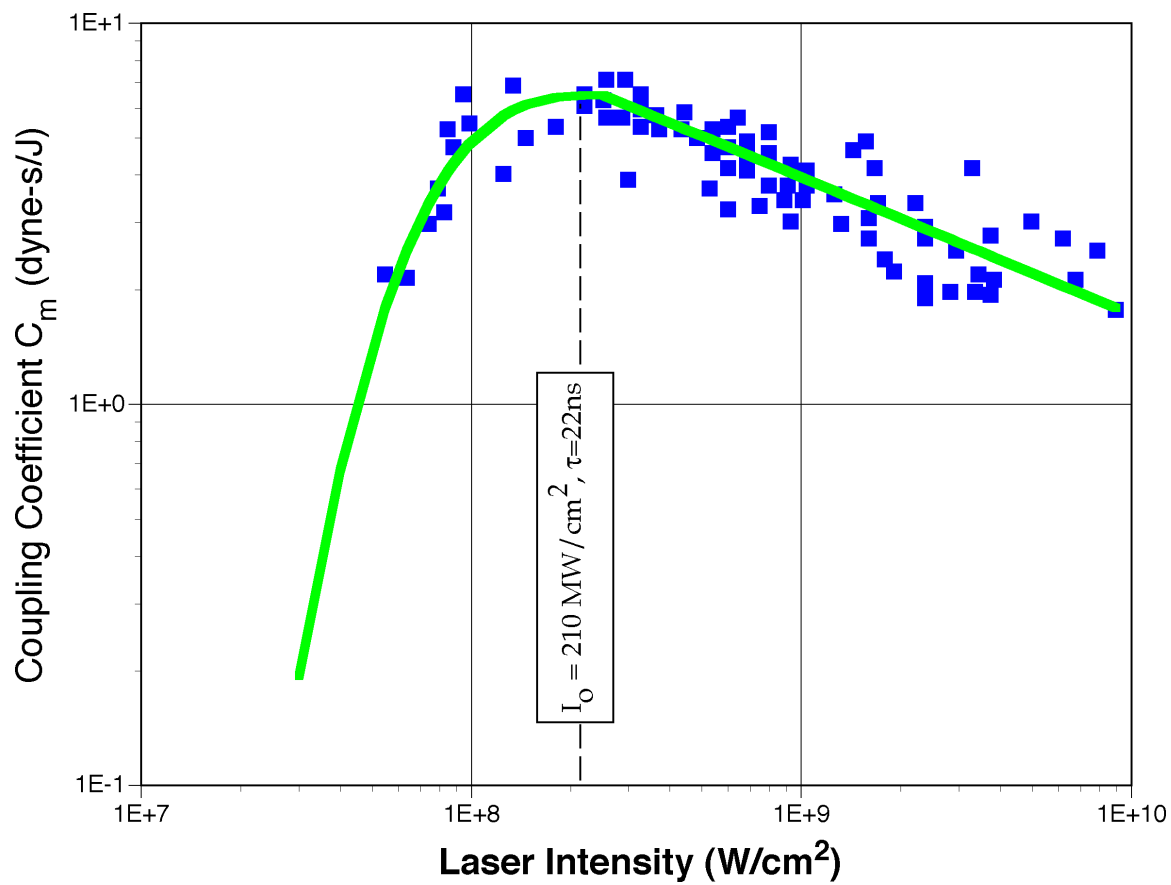


Figure A4.1: Coupling coefficient data for 22-ns KrF laser pulses on nylon in vacuum [Phipps *et al.* 1988] show the typical variation of C_m with peak pulse intensity and illustrate what is meant by “optimum coupling fluence” Φ_{opt} which, in this case, is $4.6 \text{ J}/\text{cm}^2$ [point “A” in Figure A4.2].

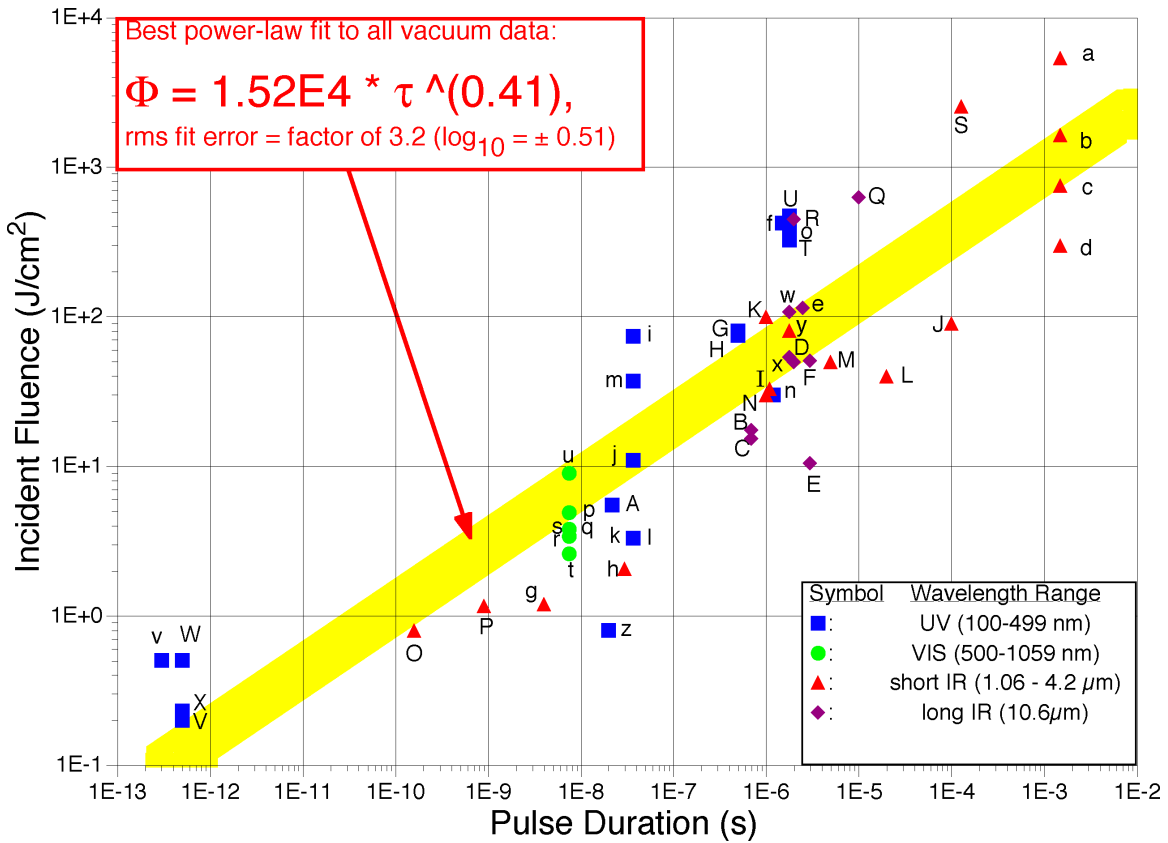


Figure A4.2. The minority of experiments reported in the literature for which the peak momentum coupling fluence Φ_{opt} was measured or can be deduced give the 51 data points shown in this Figure. Representing lasers with wavelength from 248 nm to 10.6 μm and pulse durations 300 fs < τ < 1 ms acting on metals and nonmetals, they follow a trend (the grey bar in the Figure) described by Eq. [A4.1] with $m=0.41$ and $F = 1.5E4$ to within an rms fit error of a factor of 3 at any given pulse duration. References corresponding to the points are: a,b,c,d: Afanas'ev, *et al.* 1969; e: Apostol, *et al.* 1976; f: Augustoni, *et al.* 1986; g,h: Combis, David & Nierat, 1992; i,k,l,m: Dingus, R. 1987; n: Duzy, *et al.* 1980; o: Ermer, *et al.* 1987; p,q,r,s,t,u: Gregg, D. & Thomas, S. J. 1966; v: Küper & Stuke, 1989; w,x,A: Phipps, *et al.* 1988; y: Phipps, *et al.* (unpublished); z: Dreyfus 1991; B,C: Phipps *et al* 1990; E,F: Rosen, *et al.* 1978; G: Rosen, *et al.* 1982; H: Rosen, Hastings & Weyl 1982; I, J, K, L, M, N: Rudder, R. R. 1974; O, P: Combis, *et al.* 1992; Q: Shui, Young & Reilly, 1978; R: Ursu, *et al.*, 1981; S: Watt 1987; T, U: Wilson 1986; V, W, X: Preuss, *et al.* 1995.

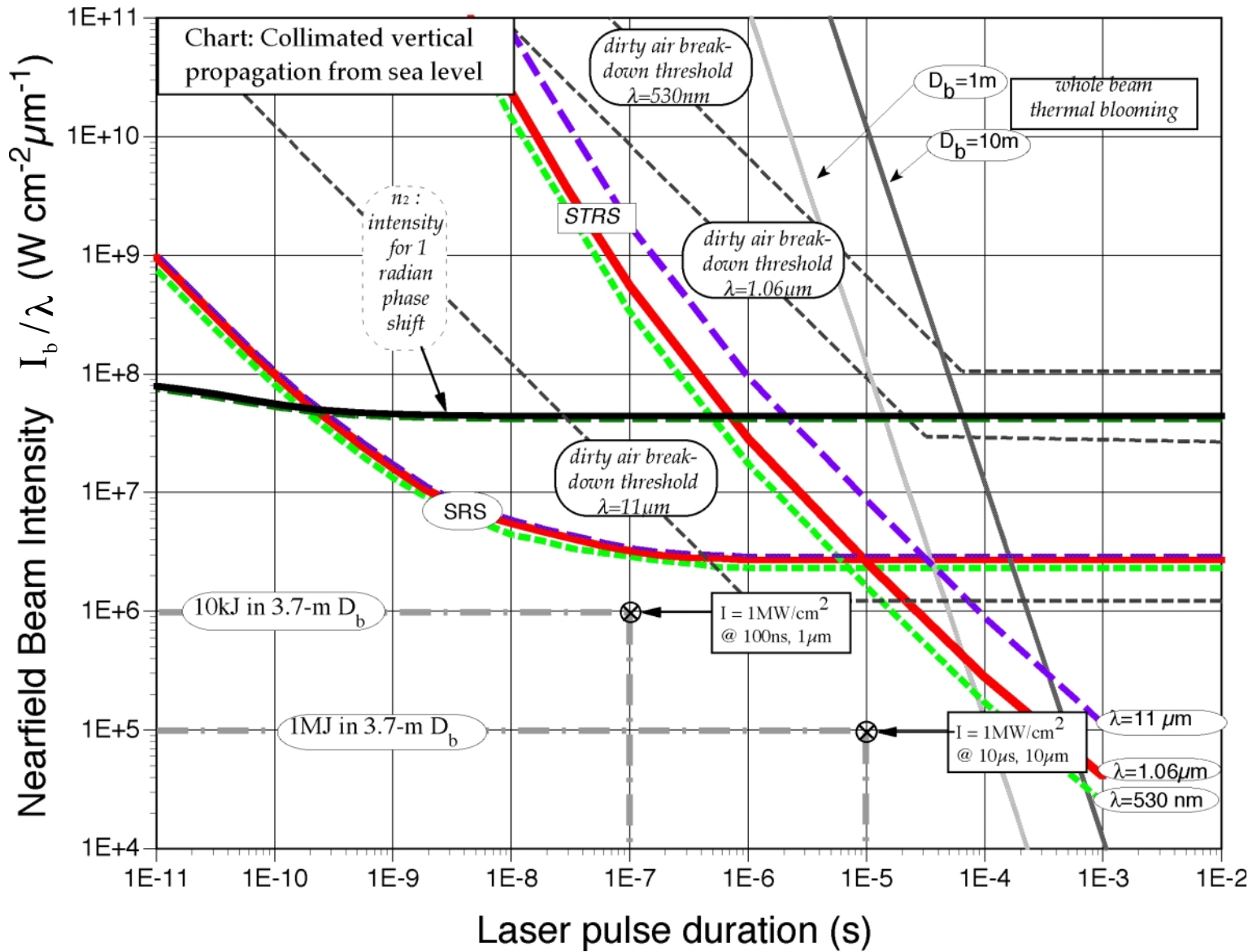


Figure A4.3. Two examples illustrate the use of the “maneuvering room” chart.

A 3.67-m-diameter telescope launches a 1- μm wavelength beam with 100-ns pulse duration from a 3.7-m-diameter aperture at $1\text{MW}/\text{cm}^2$ intensity. This intensity is safe from the nearest threatening effect, Stimulated Raman Scattering (SRS). Other effects, such as Stimulated Thermal Rayleigh Scattering (STRS), which is the wavelength-scale version of whole beam thermal blooming instability, and nonlinear index (n_2) are not significant threats. This intensity, pulsedwidth and beam diameter corresponds to 10kJ/pulse energy. The same intensity at the longer pulse duration at 10- μm wavelength gives 1MJ pulses.

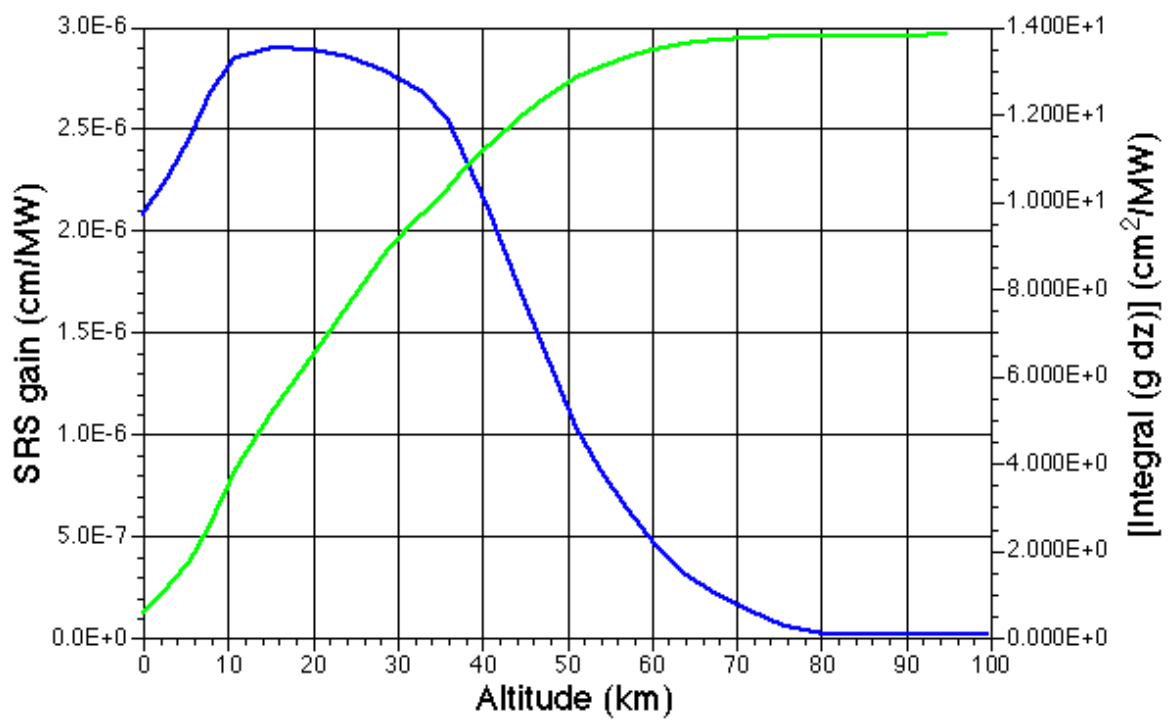


Figure A4.4 SRS gain (left-hand axis) and its integral vs. altitude for $\lambda=1\mu\text{m}$ following Kurnit *et al.* 1987

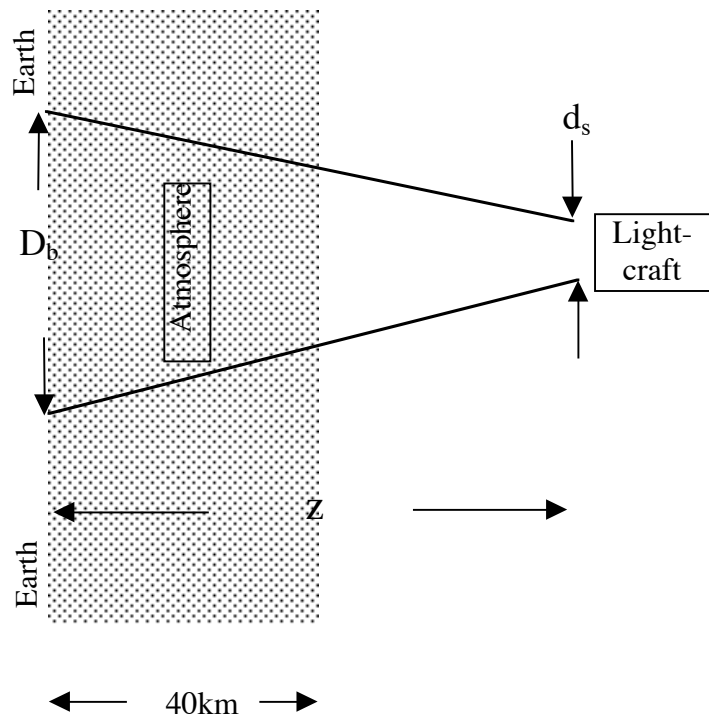


Figure A4.5 Illustrating the necessity of integrating g^*I^*dz from the source to the target. The 40km dimension shown is the effective thickness of the layer which generates SRS [see Figure A4.4], not the scale height of the atmosphere.

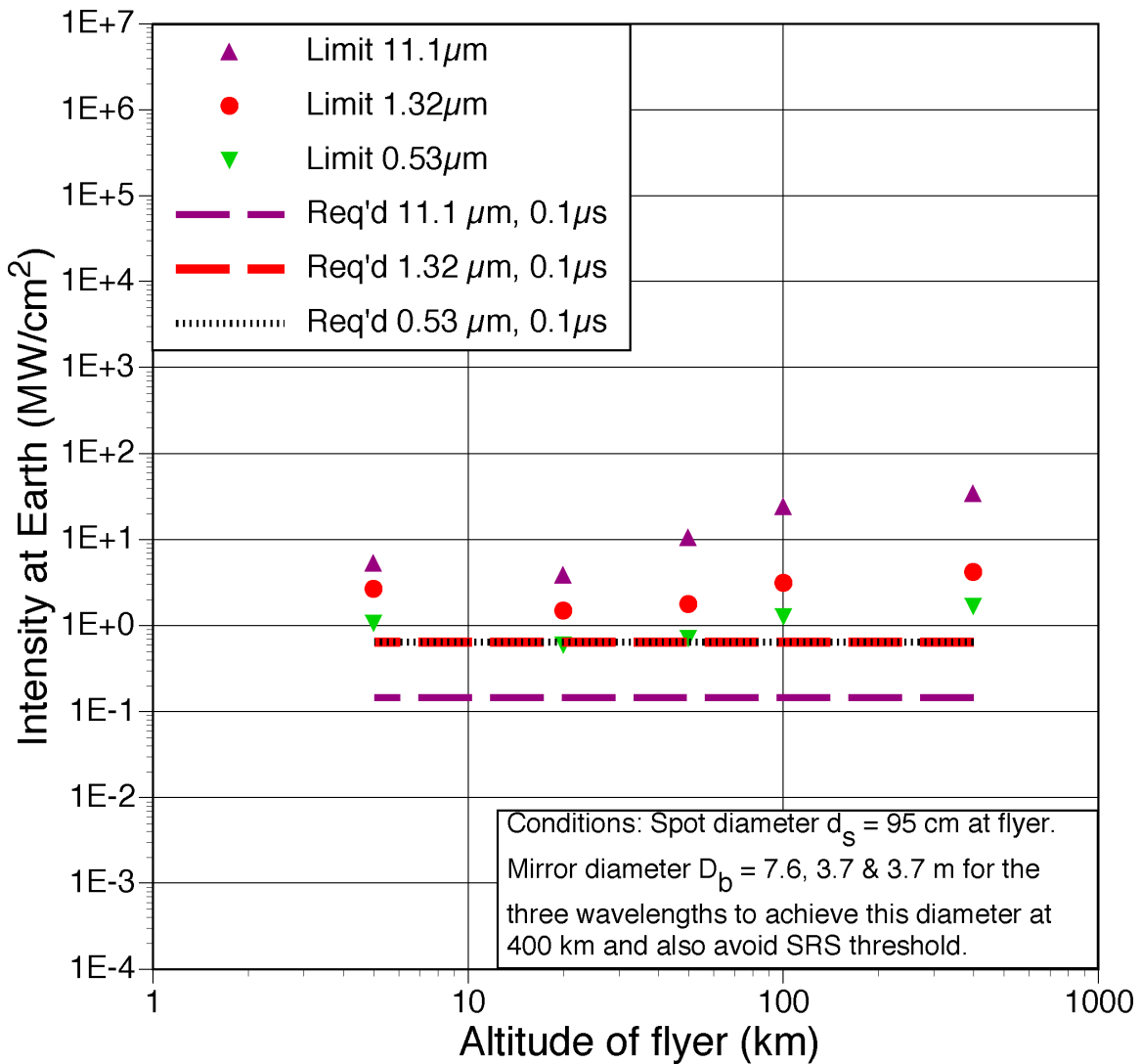


Figure A4.6: Results of calculations of maximum SRS intensity on the ground while focusing vertically through the atmosphere to a 95-cm-diameter collecting optic on flyer, showing the complex interplay of diffraction, decreasing average intensity as altitude increases, and the intensity required to achieve optimum coupling on the ablator. Mirror sizes were deliberately chosen to highlight this interplay, and were dominated by avoiding SRS rather than focusing on the distant target for this range at the two shorter wavelengths.

Table A4.1: SRS limits for the laser Lightcraft problem

Assumptions: 95-cm collecting optic, 21-cm ablator diameter, S=0.5, T=0.8.

Calculations include effect of focusing in atmosphere

Pulse-width (μs)	Wave-length (μm)	Pulse energy req'd for ablation (kJ)	Laser Rep. Rate for 1MW avg. power (Hz)	SRS threshold intensity I_{SRS} (MW/cm ²), Vertical prop. from sea level. (Worst alt. km)	SRS threshold intensity I_{SRS} (MW/cm ²), 45° zenith angle prop. from sea level. (Worst alt. km)	Telescope diameter D_b (m)	Pulse intensity I_b (MW/cm ²) req'd at Earth in a beam of diameter D_b	Vert. Prop. Safety Factor
0.1	0.53	6.8	150	0.6 (20)	0.4 (20)	3.67	0.6	1.0
1.0	0.53	19	50	0.6 (20)	0.4 (20)	3.67	1.8	0.3
0.1	1.32	6.8	150	1.5 (20)	1.1 (20)	3.67	0.64	2.3
1.0	1.32	19	50	1.5 (20)	1.1 (20)	3.67	1.8	0.8
0.1	11.1	6.8	150	17 (20)	12 (20)	7.66	0.15	110
1.0	11.1	19	50	17 (20)	12 (20)	7.66	0.42	40

Appendix V: Analysis of Launch to LEO in Vacuum

As mentioned in the text, for this analysis, we idealize flights as being composed of two separable segments: a vertical flight to near LEO altitude, with engine cutoff at time t_c , and a horizontal orbit insertion segment ending at time t_l . The two flight segments may be separated by a brief coasting interval prior to engine reignition at a turning time t_T , chosen to attain $v_r = 0$ at time t_l .

Figure A5.1 is the result of an actual orbit insertion simulation of an “elbow” flight path which demonstrates that this assumption is not unreasonable: the path shown gave a mass ratio m_I/M which was 91% of the best mass ratio obtained in any simulation in our study.

The “elbow” path is good for analysis, but [see Figures 12A and 12B of the text] impossible for a single laser station because the incidence angle goes to $\pi/2$ at the turning point. For this reason, in many of the simulations, custom-designed paths were used [see Figures 11A and 11B of the text]. This was done primarily to see how small the range of beam incidence angle on the flyer could be made during a practical flight and thereby see how practical it might be to launch a craft with just one laser station. The answer we found is summarized in Figure 17 of the text: a flight path such that incidence angle is bounded within 20° implies a path that still requires two laser stations to complete the flight because elevation angle to the craft from a single station at end of flight is unacceptably small. However, by employing the venetian blind reflectors, it is likely that an intermediate result exists with adequate incidence and elevation angle bounds. This possibility should be explored further.

For the analysis, we begin with constant ablation rate b , where the remaining mass $m(t)$ is

$$m(t) = M - b t = M - \frac{P t}{Q^*} = M \left[1 - \frac{\beta M t}{I_{sp}} \right] \quad [A5.1]$$

and the remaining ablation fuel lifetime is

$$\tau_{AB}(t) = m(t)/b \quad . \quad [A5.2]$$

For the vertical portion of the flight,

$$\ddot{x} = -\frac{\dot{m}}{m} v_E - g \quad . \quad [A5.3]$$

Integrating to the turning point (since $m_c = m_T$) we have

$$v_{rT} = \dot{x}(t_T) = -v_E \ln \left(\frac{m_T}{M} \right) - g t_T \quad , \quad [A5.4]$$

whence

$$\frac{m_T}{M} = \exp \left[- \left(\frac{v_{rT} + g t_T}{v_E} \right) \right] \quad . \quad [A5.5]$$

Since

$$\frac{m_I}{M} = \frac{m_I}{m_T} \frac{m_T}{M} \quad , \quad [A5.6]$$

we need next to determine v_{rT} and the ratio m_I/m_T for the horizontal portion of the flight, from the turning point T to insertion I.

In circular polar coordinates (Figure A5.2) the azimuthal equation of motion (EOM) is:

$$\dot{L} = m(r \dot{v}_\phi + \dot{r} v_\phi) = -\dot{m} v_E r \quad [A5.7]$$

so $-\frac{\dot{m}}{m} = \dot{\xi} \frac{\dot{r}}{r} + \dot{\xi}$ [A5.8]

$$\ln\left(\frac{m_T}{m_I}\right) = \xi_I + \int_T^I x d \ln r = \xi_I - \int_T^I \ln r d\xi + \xi_I \ln r_I = \xi_I + \epsilon \quad [A5.9]$$

where the second term has magnitude $\epsilon < 0.01$ for practical “elbow orbit” cases and may

be ignored. Accordingly, $\frac{m_T}{m} = \exp(\xi)$ [A5.10]

to good accuracy throughout the horizontal portion of the flight after time t_T and, in particular, at the end:

$$\frac{m_I}{m_T} = \exp[-(v_I/v_E)] \quad . \quad [A5.11]$$

Combining [A5.5] with [A5.11] using [A5.6] gives

$$\frac{m_I}{M} = \exp\left[-\left(\frac{v_I + g t_T + v_{rT}}{v_E}\right)\right] \quad . \quad [A5.12]$$

Now, we must find a functional form for v_{rT} . To do this, we note that the radial EOM is

$$\dot{v}_r = \omega^2 r - g = \frac{v_E^2}{r} \xi^2 - g \quad . \quad [A5.13]$$

during the horizontal portion of the flight. Integrating, and requiring that the radial velocity at insertion is zero defines the magnitude of v_{rT} :

$$v_{rI} \equiv 0 = v_{rT} - g \Delta t + \frac{v_E^2}{r} \int_T^I \xi^2 dt \quad . \quad [A5.14]$$

Rewriting [A5.10] as

$$\xi^2 = \ln^2(m_T/m) \quad ,$$

and since

$$\frac{m_T}{m} = \frac{m_T}{m_T - b t'} \quad , \quad [A5.15]$$

with

$$t' = t - t_T$$

and writing

$$u = \frac{m_T}{m_T - b t'}$$

we have

$$\int_T^I \xi^2 dt = \frac{m_T}{b} \int_{u_T=1}^{u_I=m_T/m_I} \frac{du}{u} \ln^2(u) . \quad [A5.16]$$

We can then do the integral in [A5.14] using Eq. 2.721.1 & 2.723, Gradshteyn & Ryzhik 1965:

$$\begin{aligned} \int_T^I \xi^2 dt &= \frac{m_T}{b} \left\{ -\frac{\ln^2 u}{u} \Big|_T^I + 2 \int_T^I \frac{du}{u^2} \ln u \right\} \\ &= \frac{m_T}{b} \left[-\frac{\ln^2(m_T/m_I)}{m_T/m_I} - 2 \frac{\ln(m_T/m_I)}{m_T/m_I} + 2(1 - m_T/m_I) \right] \end{aligned} \quad [A5.17]$$

Then,

$$v_{rT} = g \Delta t + \frac{v_E^2 m_I}{b r} \left[\ln^2(m_T/m_I) + 2 \ln(m_T/m_I) - 2(m_T/m_I - 1) \right] . \quad [A5.18]$$

where $\Delta t = (t_I - t_T)$ is the duration of the horizontal flight. Equating Eqn. [A5.18] with Eqn. [A5.4] gives a transcendental equation from which v_{rT} can be determined, in principle. First, we obtain a value for $\zeta = (m_T/m_I)$ by iterating this relationship:

$$-v_E \ln \left(\frac{m_I}{M} \zeta \right) = gt_I + \frac{v_E^2 m_I}{b r} \left[\ln^2 \zeta + 2 \ln \zeta - 2(\zeta - 1) \right] \quad [A5.19]$$

starting with a value for v_E and progressively improving guesses for m_I/M and m_I/b . Then, this value is inserted into [A5.18] to actually evaluate v_{rT} .

However, we are now in a position to evaluate the numerator in the exponential of Eq. [A5.12].

$$\begin{aligned} v_I + g t_T + v_{rT} &= v_I + g t_T + g t_I \pm g t_T + v_E \ln \Gamma \\ &= v_I + g t_I + v_E \ln \Gamma \end{aligned} \quad [A5.20]$$

Accordingly, the answer we have been seeking is:

$$\frac{m_I}{M} = \Gamma \exp \left[-\left(\frac{\Delta v + gt_I}{v_E} \right) \right] , \quad [A5.21]$$

as stated in Eq. [12] of the text.

The parameter Γ is

$$\Gamma = \exp \left\{ -\frac{v_E m_I}{b r} \left[\ln^2 \zeta + 2 \ln \zeta - 2(\zeta - 1) \right] \right\} \quad [A5.22]$$

We evaluated ζ using [A5.19] for practical “elbow orbit” cases for LEO where $t_I \leq 1000$ s, $\beta \geq 1$ and $3E5 \leq v_E \leq 5E6$ cm/s and determined that the function $\Gamma(\zeta)$ is always in the range $1.0 \leq \Gamma < 1.02$ [Table A5.1]. Therefore, Γ may be ignored for the purposes of this analysis, as stated in the text.

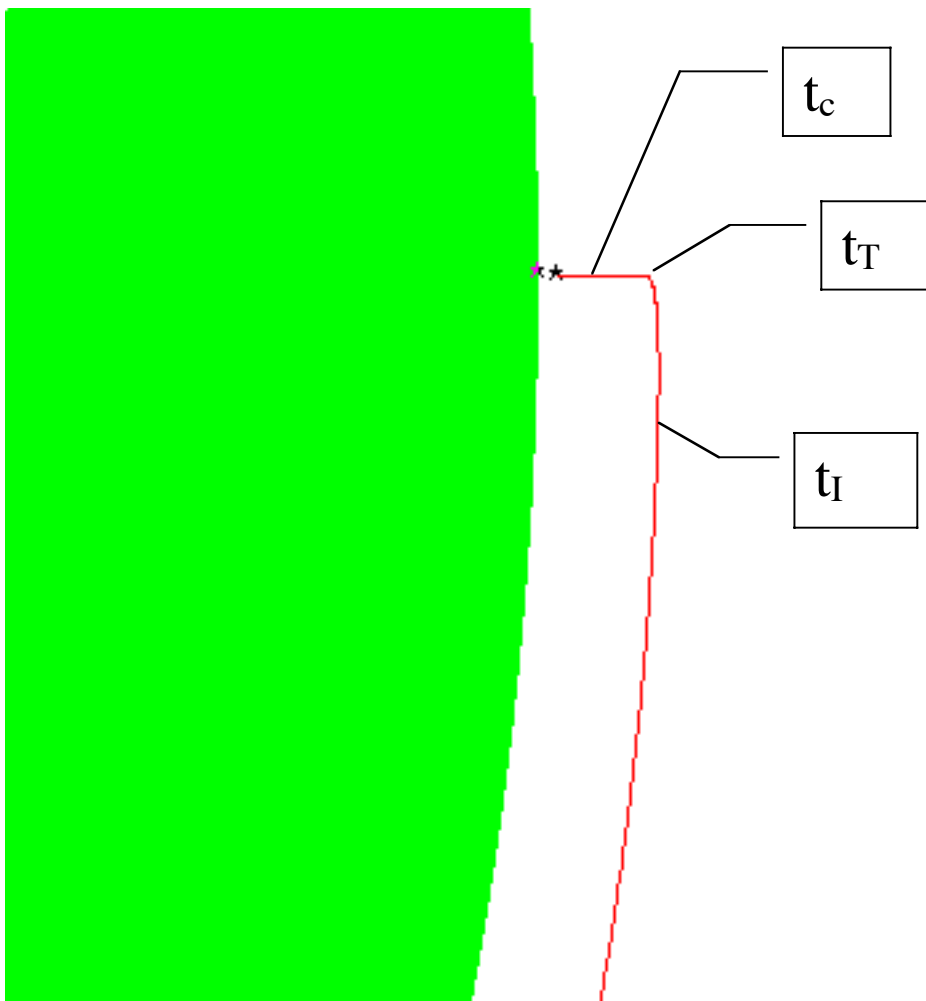


Figure A 5.1 Actual path of simulated “elbow” flight, demonstrating that the type of path used for analytical work corresponds closely to reality. Conditions: $x_o = 30$ km, $C_m=20$, $v_E = 10$ km/s, $\beta = 4$, $P = 1.96$ MW, $M = 10$ kg, $v_{rT} = 0.65$ km/s, $t_c = 79$ s, $t_T = 168$ s, $m_T = 6.36$ kg, $m_I = 2.91$ kg and $t_I = 257$ s. Result: $m/M = 91\%$ of the best result obtained with a hand-built orbit insertion path (Table 6 of text).

Flyer

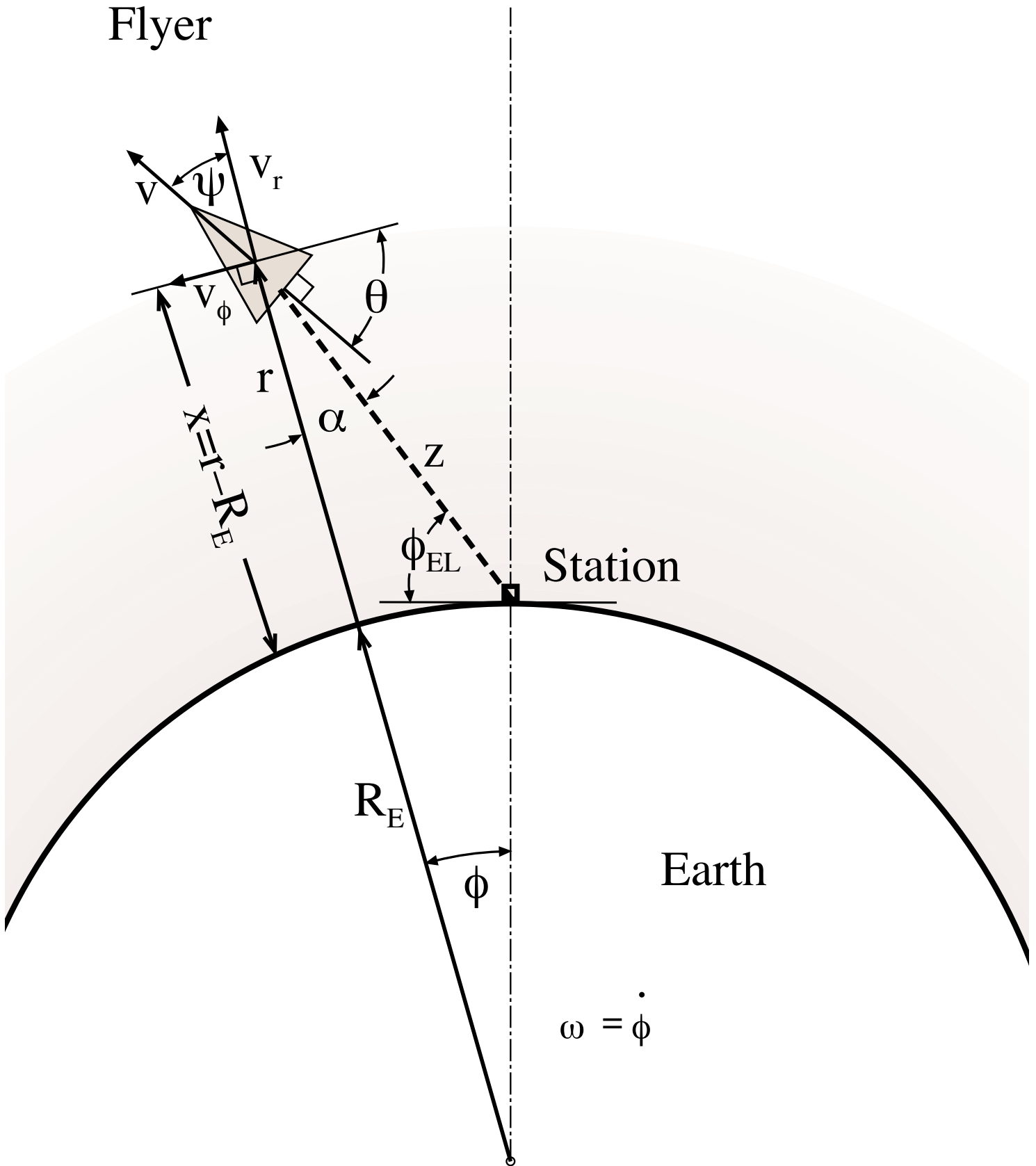


Figure A5.2. Geometry for Flight Analysis

Table A5.1: Numerical Results for ζ

[Determined from Eq. (A5.19) with $\beta \geq 1$ and $t_l < 1000s$]

v_E	$\zeta = m_T/m_I$	Γ
5E+6	1.2	1.008
2E+6	1.2	1.002
1E+6	2.0	1.014
5E+5	4.4	1.019
3E+5	9.0	1.010